Rivers, reefs, and deltas; Geomorphological evolution of the Jurassic of the Farsund Basin, offshore southern Norway

Thomas B. Phillips*[1], Christopher A-L. Jackson, Rebecca E. Bell, Ayunda A. Valencia

Basins Research Group (BRG), Department of Earth Science and Engineering, Imperial College, South Kensington Campus, Prince Consort Road, London, SW7 2BP, UK

[1]Now at Department of Earth Science, Durham University, Science Labs, Durham, DH13LE

*Corresponding author: tbphil13@gmail.com

Abstract

In many petroleum-bearing, data-poor ‘frontier’ basins, source, reservoir, and seal distribution is poorly constrained, making it difficult to identify petroleum systems and play models. However, 3D seismic reflection data provide an opportunity to directly map the three-dimensional distribution of key petroleum system elements, thereby supplementing typically sparse, one-dimensional sedimentary facies information available from wells. Here, we examine the Farsund Basin, an underexplored basin offshore southern Norway. Despite lying in the mature North Sea basin, the Farsund Basin contains only one well, meaning there remains a poor understanding of its hydrocarbon potential. This E-trending basin is anomalous to the N-trending basins present regionally, having experienced a different tectonic, and likely geomorphological, evolution. We identify a series of east-flowing rivers in the Middle Jurassic, the distribution of which are controlled by salt-detached faults. In the Middle Jurassic, a series of carbonate reefs, expressed as sub-circular amplitude anomalies, developed. Within the Upper Jurassic we identify numerous curvilinear features, which correspond to the downlap termination of southwards-prograding deltaic clinoforms. We show how seismic-attribute driven analysis can determine the geomorphological development of basins, offering insights into both the local and regional tectono-stratigraphic evolution of an area and helping to determine its hydrocarbon potential.

1 Introduction

Successful hydrocarbon exploration requires a knowledge of how sedimentary basins evolve in terms tectonic events and depositional patterns, and how this leads to the development of working petroleum systems and plays (e.g. Johannessen & Andsbjerg 1993; Posamentier 2004; Dreyer et al. 2005; Holgate et al. 2013). Predicting the occurrence of source, reservoir and source rocks is a critical element of petroleum systems analysis, although this is especially challenging in frontier or underexplored basins due to a lack of well data. Even where available, these well data provide only one- to quasi-three-dimensional constraints on the distribution of various rock types in the subsurface. Outcrop studies may provide detailed insights into the typical geometries and spatial relationships between different facies types, but they do not replicate specific subsurface geometries (e.g. Prélat et al. 2009; Romans et al. 2011; Agirrezabala et al. 2013; Holgate et al. 2014; Legler et al. 2014). Therefore, our understanding of the geological complexity of an area, including the distribution of different rock types and constituent petroleum systems, is heavily influenced by well spacing, reducing the accuracy and resolution of derived play maps and tectono-stratigraphic models (e.g. Johannessen & Andsbjerg 1993; Dreyer et al. 2005; Holgate et al. 2013; Mannie et al. 2014). These issues are particularly relevant in underexplored areas where a complex area, with a relatively localised geological evolution, may not be incorporated into regional models due to a lack of data and low resolution.

High-quality 3D seismic reflection data does not always suffer from such spatial aliasing, providing relatively high-resolution images (10’s m) of ancient geomorphic landscapes and seascapes preserved in the Earth’s subsurface. By using amplitude and frequency derived seismic attributes, such as root mean square (RMS) amplitude, variance, dominant frequency, and spectral decomposition, we are able to constrain, to varying degrees

of confidence, the geometry and distribution of different rocks types within the subsurface (e.g. Ryseth et al. 1998; Posamentier & Kolla 2003; Posamentier 2004; Colpaert et al. 2007; Chopra & Marfurt 2008; Jackson et al. 2010; Zhuo et al. 2014; Klausen et al. 2016; Eide et al. 2017). Using 3D seismic reflection data we can therefore examine the stratigraphic evolution of the subsurface over a greater areal extent than borehole data, albeit often at a coarser temporal resolution (e.g. Cartwright & Huuse 2005; Colpaert et al. 2007; Jackson et al. 2010; Jackson & Lewis 2013; Klausen et al. 2016; Saqab & Bourget 2016). Seismic geomorphological analysis can therefore also provide additional context to the geological evolution of an area, helping to reduce exploration risk and to update regional tectono-stratigraphic models in frontier or underexplored areas.

Here, we conduct a seismic attribute-driven interpretation of 2D and 3D seismic reflection data located offshore southern Norway, and analyse the 3D facies architecture of the Triassic and Jurassic section preserved in the relatively underexplored Farsund Basin (Figure 1). Data from well 11/5-1, located along the southern margin of the basins, provides independent constraints on the lithology of the depositional elements imaged within the 3D seismic volume (Figure 1). Current paleo-geographical models within this area are largely based on regional borehole-correlation studies, with data primarily from the adjacent Egersund and Norwegian-Danish Basins and little within the Farsund Basin; these studies document a clastic-dominated net-transgressive setting throughout the Jurassic (Sørensen et al. 1992; Mannie et al. 2014; Mannie et al. 2016). However, the tectonic evolution of the Farsund Basin differed to that experienced by adjacent basins, being heavily influenced by activity along the underlying lithosphere-scale Tornquist zone (Phillips et al. 2018). Here, we investigate whether this contrasting tectonic history resulted in a unique stratigraphic record and petroleum systems, unlike those encountered in nearby basins.

By undertaking detailed seismic geomorphological analysis and seismic attribute-driven interpretation, we constrain the geomorphological evolution of the Farsund Basin throughout the Jurassic, identifying a series of fluvial systems, carbonate patch reefs and shallow marine deltaic lobes. We compare and contrast our observations of the geomorphological evolution of this area to the regional stratigraphic framework (Figure 1b), providing insights into and further constraining the tectonics, sedimentation history and hinterland character of the basin and wider region.

2 Regional geological setting

This study focusses on the E-trending Farsund Basin, located offshore southern Norway (Figure 1). To the north and south, the basin is bordered by the Permian-Carboniferous aged Varnes Graben and Norwegian-Danish Basin, respectively (Figure 1) (Heeremans & Faleide 2004; Heeremans et al. 2004), and to the west by the much-explored Permian-Carboniferous Egersund Basin. The structural (e.g. Mogensen & Jensen 1994; Sørensen & Tangen 1995; Jackson et al. 2013; Jackson & Lewis 2013; Tvedt et al. 2013) and stratigraphic evolution (e.g. Sørensen et al. 1992; Mannie et al. 2014; Mannie et al. 2016) of the Egersund Basin has been studied by numerous authors. It is separated from the Farsund Basin by the Stavanger Platform and Lista Nose Fault Blocks (Hamar et al. 1983; Skjerven et al. 1983; Jackson & Lewis 2013; Lewis et al. 2013) (Figure 1). To the east, the Farsund Basin opens into the Norwegian-Danish Basin and Sorgenfrei-Tornquist fault complex (Nielsen 2003; Heeremans et al. 2004; Olivarius & Nielsen 2016).

The southern margin of the Farsund Basin is defined by the N-dipping Fjerritslev Fault system (Figure 1), which within the 3D seismic volume comprises the Fjerritslev North and Fjerritslev South Faults (Figure 2a). A further E-W striking fault, the Farsund North Fault

is located outside of the 3D volume and forms the northern margin to the basin (Figure 1). A series of N-S-striking faults are present across the southern margin of the basin; the two largest of which control the preservation of Triassic strata and are termed NS1 and NS2 to the north and south of the Fjerritslev North Fault, respectively (Figure 2a). At shallower stratigraphic levels, N-S striking faults are largely absent, with the basin morphology controlled by the E-W striking Fjerritslev North and South faults (Figure 2b, c).

A detailed analysis of the structural evolution of the Farsund Basin can be found in Phillips et al. (2018), which we here review in the context of the North Sea basin development. Prior to its formation, the proto-Farsund Basin was located along the northern margin of the North Permian Basin, which contained mobile evaporites of the Upper Permian Zechstein Supergroup (Christensen & Korstgård 1994; Heeremans et al. 2004; Jackson & Lewis 2013). The Triassic was associated with regional E-W extension, leading to activity along N-S striking faults, such as NS1 and NS2, across the study area (Figure 2c). Widespread uplift and erosion occurred across large parts of the Central North Sea during the Middle Jurassic in response to uplift of the Mid-North Sea thermal dome (Rattey & Hayward 1993; Underhill & Partington 1993). To the east, this resulted in the erosion of Triassic-to-Lower-Middle Jurassic strata and the formation of the BJU across the study area (Figure 3). A regional rift phase is documented across the North Sea from the Late Jurassic-to-Early Cretaceous (Ziegler 1992; Færseth 1996; Coward et al. 2003), which led to the formation of the E-W striking faults, i.e. the Fjerritslev North and South Faults and the Farsund North Fault that define the present-day morphology of the Farsund Basin (Figure 1, 2a) (Mogensen & Jensen 1994; Sørensen & Tangen 1995; Phillips et al. 2018).

3 Dataset and methodology

Seismic interpretation was primarily undertaken on a 500 km^2 3D seismic reflection dataset located across the southern margin of the Farsund Basin (Figure 1). These data image to 4 seconds two-way-time (TWT) (c. 6 km) with inline and crossline spacings of 18.75 m and 12.50 m, respectively. Frequency values were measured throughout the interval of interest (0.75-1.30 s TWT) and range from 25-40 Hz, with a mean frequency of ~35 Hz (Figure 4). Using an average velocity of 2.5 kms^{-1} for the overlying sedimentary cover (based on well 11/5-1), corresponding values of vertical resolution ($\lambda/4$) range from 15 to 25 m (Figure 4a). Based on an average frequency of ~35 Hz we determine an average vertical resolution ($\lambda/4$) of ~18 m and an average limit of detectability ($\lambda/30$) of ~2 m (Widess 1973; Kallweit & Wood 1982; Slatt 2006).

Additional seismic interpretation was undertaken on a series of N-S oriented 2D seismic sections (Figure 1), which image to 7 s TWT (c. 15 km) and allow interpretation of the stratigraphic horizons over a wider area, providing a more regional perspective to our interpretations. Seismic data are displayed as zero phase and follow the SEG normal polarity convention; that is, a downward increase in acoustic impedance is represented by a peak (black), and a downward decrease in acoustic impedance is represented by a trough (red) (Figure 3). The ages of key stratigraphic horizons are constrained through a number of wells regionally (Figure 1). Well 11/5-1, the only well located within the 3D seismic volume (Figure 2), provides detailed 1D facies information within the study area and is tied to the seismic interpretations through a seismic-well tie (Figure 5). The synthetic seismogram proves a good fit to the seismic data in areas where both sonic and density logs are available, with a good match between the top Rotliegend and top Sandnes horizons, and the lower section of the Egersund Formation (Figure 5). There is a poor fit throughout the Egersund and

Tau Formations that is primarily related to a lack of density log information in the interval 1130-1180 m. Areas immediately above and below this data-absent interval, and towards the top of the log, where data recording begins, are influenced by edge effects relating to data-absent areas and therefore poorly correlate with the original seismic trace (Figure 5). Seismic attributes, such as RMS amplitude, variance, dominant frequency, and spectral decomposition were calculated within windows located either above, below or between specific key horizons in order to further interrogate and extract information from the seismic data (see Appendix A for details regarding specific seismic attributes).

We used GeoTeric software in order to calculate the spectral decomposition attribute. To do this, we extracted a frequency spectrum from the data and split this into a series of discrete bins, each corresponding to a range of 10 Hz (Figure 4). Frequency values centred on 22, 30 and 45 Hz were assigned to the colours red, green and blue, respectively and blended to produce the spectral decomposition attribute (Figure 4b).

4 Regional stratigraphy

We here describe the stratigraphic succession preserved in the Farsund Basin as revealed by well 11/5-1, and compare it to the succession encountered regionally (Figures 1, 2, 5). The Triassic interval is non-marine succession across the much of the North Sea (McKie & Williams 2009; Jarsve et al. 2014). Triassic strata are preserved within the footwalls of the NS1 and NS2 faults, although no Triassic strata are encountered in well 11/5-1, with Middle Jurassic strata unconformably overlying the Upper Permian Rotliegend Group due to erosion by the BJU (Figure 3, 5). The Middle Jurassic (Bajocian-Bathonian) Bryne Formation is present regionally, but is also not present in well 11/5-1 (Figure 5). The Bryne Formation in the adjacent Egersund Basin comprises non-marine sandstone and siltstone

(Vollset & Doré 1984; Mannie et al. 2016). Stratigraphically above the Bryne Formation, and forming the lowermost Jurassic interval penetrated in well 11/5-1, is the Mid-Jurassic (Callovian) Sandnes Formation. In well 11/5-1 this is comprised of 45 m of predominantly marine sandstones and mudstones, with some intervals containing abundant m-scale carbonate stringers (Figure 5) (Vollset & Doré 1984; Mannie et al. 2016). The Late Callovian-to-Early Tithonian Egersund and Tau formations are situated stratigraphically above the Sandnes Formation. These formations make up the majority of the Jurassic interval in well 11/5-1 (189 m) and consist of organic-rich claystones and shales (Figure 5). Isolated glauconitic and pyritic layers are present throughout these formations, indicating a low-energy depositional environment that was prone to anoxic conditions (Figure 5) (Vollset & Doré 1984). Regionally, the uppermost Jurassic (Tithonian) to lower Cretaceous Sauda Formation consists of marine shales. However, in well 11/5-1, the upper 15 m of the 22 m thick Sauda Formation (incorporating the lowermost Lower Cretaceous interval) is sandstone-dominated (Figure 5). The Jurassic interval in both the Farsund Basin and regionally is overlain by a large thickness of Lower Cretaceous deepwater claystones and mudstones.

5 Seismic geomorphological observations and interpretation

Well 11/5-1 provides direct constraints, albeit only in one dimension, on the stratigraphy of the Triassic and Jurassic succession of the Farsund Basin. Using this stratigraphic framework, we now use a suite of seismic attributes (see Appendix A) to determine the 3D geometry and distribution of different facies types within the basin. In each subsection, we first describe our seismic geomorphological observations, based on seismic reflection, seismic attribute and well data analysis before posing an interpretation for the likely depositional environment and geomorphological origin of the identified features.

5.1 Triassic – Limit of thin-skinned tectonics and depositional extent of mobile Zechstein salt

In the North Permian Basin, Zechstein salt is overlain by Triassic strata (Clark et al. 1998; Lewis et al. 2013). Post-depositional salt mobilisation and modification means that the initial depositional limit of salt and salt basins is often uncertain (Clark et al. 1998; Jackson & Lewis 2013). Triassic strata in the Farsund Basin are dominated by S-dipping, salt-detached normal faults, related to southwards directed salt-mobilisation into the Norwegian-Danish Basin (Figure 6). The top of the Triassic interval is eroded by the BJU, with Triassic strata largely absent across the footwalls of NS1 and NS2, north of the Fjerritslev South Fault (Figure 3, 5). The Fjerritslev North and South Faults in this area do not show any pre-Cretaceous activity and were not present during the Triassic, with the Fjerritslev South Fault appearing restorable up to the BJU (Figure 3, 6) (Phillips et al. 2018).

Within the hanging wall of the Fjerritslev South Fault, a series of small-scale (c. 50 ms TWT, 70 m height) clinoforms are identified in the Triassic interval, prograding towards the south (Figure 6). The relatively small height of these clinoforms, and the sub-aerial regional character of the Triassic (Jarsve et al. (2014), implies deposition within a terrestrial,

likely fluvio-deltaic environment (cf. Patruno et al. 2015a). Immediately south of these clinoforms, now located on the footwall of the Fjerritslev South Fault, thin-skinned salt-detached faulting is restricted northwards (Figure 6). We propose that the transition from the preserved clinoform sequence in the north, to where the clinoforms are bisected by thin-skinned salt-related faults in the south could indicate the initial northern depositional limit of the mobile component of the Zechstein salt (Figure 6). North of this limit, mobile Zechstein salt, or salt of sufficient thickness to flow, is not present. We propose the following model; prior to salt mobilisation, deltaic clinoform sequences prograded southwards over the Zechstein salt basin (Figure 6). Following the onset of salt mobilisation during the Triassic, areas with underlying Zechstein salt were subject to the formation of thin-skinned salt-detached faults, offsetting shallower strata, including the clinoform sequence. However, areas north of the initial depositional limit, where no salt was present or was unable to flow, were unaffected and preserve the southwards prograding clinoform-bearing sequences (Figure 1, 6). Using these criteria we are able to map the original depositional limit of mobile Zechstein salt across the present-day Farsund Basin. The depositional limit strikes E-W across the footwall of the Fjerritslev South Fault, which had not formed at that time (Figure 1). Further east, the depositional limit of the Zechstein salt steps northwards across NS2, indicating that some relief may have been present across this fault during salt deposition, before continuing in an E-W orientation to the east (Figure 1).

5.2 Bryne Formation – Fluvial systems

In the footwall of the Fjerritslev South Fault we identify two high-amplitude, laterally discontinuous reflections above the BJU (Figure 7). Additional features may be present elsewhere in the basin, but are not identifiable due to overall high reflectivity through much of this succession. The high-amplitude reflections are situated in the hanging walls of thin-skinned, salt-detached faults (Figure 7). Each feature is around 500 m wide and is imaged as

a very high-amplitude, tuned seismic reflection, making it difficult to calculate their true thickness (Figure 3, 7) (Widess 1973; Brown 2011). However, given that the vertical resolution of the data in this interval is ~24 m (Figure 4a), this value represents a maximum thickness estimate. Due to the restricted lateral extent of these reflections, and their stratigraphic position below the Sandnes Formation, we interpret these features are not penetrated by well 11/5-1 and instead correspond to the Bryne Formation, thereby representing the oldest Jurassic strata in the Farsund Basin.

We extract RMS amplitude, variance and dominant frequency seismic attributes, calculated within a 25 ms TWT window above the top of the BJU horizon in order to encompass the full thickness of the features, highlight their 3D geometry and provide clues as to their geological origin (Figure 7). In map view, the RMS amplitude attribute highlights two E-W trending high-amplitude features, with curvi-linear channel-like geometries, on the footwall of NS2, termed Channel 1 and Channel 2 from north to south, respectively (Figure 8). Channel 1 is ~8 km long and can be traced westwards across the footwall of the Fjerritslev South Fault. It is not imaged in the hanging wall of the Fjerritslev South Fault, due to the amplitude signal being masked by higher background amplitudes (Figure 8). Channel 2 originates within the footwall of the Fjerritslev South Fault, has an overall length of ~9 km, and widens eastwards from c. 200 m to c. 400 m (Figure 8). In cross-section the channels display an asymmetric geometry, with Channel 2 being thicker towards the south (Figure 7). Both channels cross, and are not offset by, NS2 to the east (Figure 8). However, the channels widen as they cross NS2, from c. 500 m in the footwall to c. 2 km in the hanging wall. Furthermore, the channels display a more SE orientation within the footwall of the fault (Figure 8).

The variance and dominant frequency seismic attributes provide more detailed insights into the channel geometry. The variance attribute highlights a series of minor linear

channels oriented perpendicular to, and joining along both channel 1 and 2. These secondary channels display lengths and widths of ~400 m and ~150 m, respectively (Figure 8c). In some instances these minor channels link Channel 1 and Channel 2 ('linking channel' on Figure 8e). The secondary channels display an asymmetric distribution with respect to the main channel, being concentrated along one margin, which displays a relatively shallow gradient. The opposite margin of the channel is more sharply defined and is often associated with an underlying salt-detached fault (Figure 7, 8). The dominant frequency attribute further defines the first-order geometry of the channels within the footwall of NS2, which are delineated by relatively high frequencies (~45 Hz along the margins of the channels and ~35 Hz in the centre).

Based on the seismic attribute-derived observations described above, we interpret these channel-like features as originally E- to SE-flowing, Middle Jurassic fluvial systems within the Bryne Formation. The high-amplitude character of the channels indicates a different, perhaps more sand-prone, lithology to the Egersund and Sandnes formation mudstone above and potentially fine-grained lithologies below (Figure 5, 7). The smaller structures merging along the margins of the main channels are interpreted as tributaries (Figure 8e). The E-W orientation of the channels is partly controlled by underlying thin-skinned, salt-detached faults. The underlying faults appear associated with a more sharply-defined channel margin that hosts a few tributaries, whereas the adjacent margin is associated with a gentler gradient and hosts numerous tributaries (Figure 8e). This asymmetric geometry indicates that, at least in the west, movement along these thin-skinned faults influenced the depositional surface and channel physiography. The channels were unaffected by the Fjerritslev South Fault, as this was not present at the time. Towards the east the channels widen across a topographic gradient located above NS2. This topographic gradient formed due to differential compaction of Triassic strata across the now inactive fault (Figure 8). The

widening of the channels appears to represent an estuarine setting, transitioning from a non- to shallow-marine environment. This indicates that the location of NS2 likely represented the paleo-shoreline during the deposition of the Bryne Formation in the Middle Jurassic.

5.3 Sandnes Formation – Patch reef development

Atop the Bryne Formation channel systems, a series of isolated high-amplitude features (IHAFs) are identified within a stratigraphic interval corresponding to the Middle Jurassic Sandnes Formation, which overlies the BJU and, where present, the Bryne Formation. As penetrated in well 11/5-1, the Sandnes Formation consists of sandstone and mudstone, with some isolated carbonate stringers also present. No IHAFs are directly penetrated by the borehole (Figure 5).

In cross-section, the IHAFs display a double (peak-trough) reflection character, with a large positive impedance contrast at the top (Figure 9). Two distinct IHAF morphologies are identified; short, wide structures with heights of 25 ms TWT (c. 30 m), and taller, narrower structures with typical heights of 35 ms TWT (c. 50 m) (Figure 9). The plan-view morphology of the IHAFs is further highlighted by seismic attributes (Figure 10). RMS amplitude, variance and dominant frequency attributes were extracted from a 50 ms window above the BJU and also above the Bryne Formation channels, ensuring coverage of the full height of the structures and a lack of input from stratigraphically lower features. In map-view the IHAFs are expressed as circular to sub-circular high amplitude anomalies, consisting of a high amplitude core and relatively low amplitude margin (Figure 10). A total of 333 IHAFs are identified across the area; smaller IHAFs are most accurately delineated using the spectral decomposition attribute (Figure 10c). The larger structures have a diameter or c. 450 m; whilst the smaller structures have a diameter of c. 150 m (Figure 9, 10). The tall, narrow IHAFs are predominately situated within the hangingwall of NS2, whereas the short, wide

IHAFs are restricted to the footwall (Figure 10d). Notably, the distributions of the two different morphologies are unaffected by the E-trending Fjerritslev North and Fjerritslev South faults that dominate the present-day basin morphology but were not present during the deposition of the Sandnes Formation with the wider, shorter IHAFs situated on both the hanging walls and footwalls of the Fjerritslev North and South faults (Figure 10). The distribution of the IHAFs does not change laterally to the south and west, indicating that the IHAF domain may extend outside of the 3D volume. However, the concentration of the IHAFs does decrease to the NE, in the hanging wall of both NS2 and the Fjerritslev North Fault, implying that this may represent a limit to the IHAF domain (Figure 10).

In some instances the IHAFs are cross-cut by later faults (Figure 10d, f), implying that they are brittle in nature. Some IHAFs display non-rounded, more elongate geometries, which RMS amplitude shows is typically a result of these IHAFs containing multiple high amplitude nuclei. The typical sub-rounded morphology of the IHAFs implies a radial mode of growth, with those IHAFs that contain multiple nuclei representing IHAFs that have grown radially and since merged (Figure 10e).

A variety of different processes can lead to the formation of sub-circular structures in seismic reflection data (Stewart 1999), including volcanic edifices (both igneous and mud-related) (Davies & Stewart 2005), hydrothermal vent systems (Magee et al. 2016), gas accumulations and pockmarks (Hovland et al. 1987; Fichler et al. 2005; Andresen et al. 2011; Agirrezabala et al. 2013; Marcon et al. 2014), carbonate reefs (Posamentier & Laurin 2005; Rosleff-Soerensen et al. 2012; Saqab & Bourget 2016) and evaporite structures (Jackson & Talbot 1986). Based on the relatively small (100's m scale) scale of the structures, coupled with a lack of igneous activity within this area at this time, we discount an igneous/volcanic edifice related origin for the IHAFs. Similarly, the small-scale of the IHAFs, and the lack of regional igneous activity also discounts an origin as hydrothermal vent systems (Magee et al.

2016). In addition, we do not consider an evaporate-related origin based on the IHAFs being located stratigraphically above the Upper Permian Zechstein salt, and there being no Jurassic salt present in this area of the North Sea (Jackson & Lewis 2013). Furthermore, the IHAFs are also present north of the aforementioned depositional limit of the Zechstein salt (Figure 1, 6). The relatively small-scale nature of the structures would be consistent with an origin as pockmarks; however, the structures are associated with positive relief whereas pockmarks would typically form cavities infilled with material from overlying strata (Hovland et al. 1987; Agirrezabala et al. 2013; Kluesner et al. 2013; Marcon et al. 2014).

Therefore, based on: i) their radial growth mode; ii) the positive impedance contrast at the top of the structures; iii) their overall size and morphology, along with the binary nature of the size distribution potentially reflecting different growth conditions; and iv) their brittle nature, we interpret that the IHAFs represent a series of carbonate patch reefs. Carbonate is present locally, as demonstrated by the carbonate-rich intervals penetrated in well 11/5-1 (Figure 5). Modern-day carbonate patch reefs are typically found within shallow marine environments and are often associated with sheltered low-energy environments. Modern patch reefs have diameters of c. 200 m, and heights of c. 10 m, similar to those within the study area (e.g. Brock et al. 2008; Purkis et al. 2015). The binary size distribution of the IHAFs may reflect growth conditions in slightly different, albeit still shallow, water depths. The IHAFs in slightly deeper water grow preferentially upwards towards the sea surface, compared to the wider, shorter patch reefs located in shallower waters, which have limited accommodation space and therefore grow laterally (Kendall and Schlager 1981; Schlager 1981). Carbonate patch reefs have previously been identified on seismic reflection data, displaying similar geometries, morphologies and seismic character to the IHAFs identified here (Posamentier & Laurin 2005; Ruf et al. 2008; Rosleff-Soerensen et al. 2012; Saqab & Bourget 2016). No larger-scale atolls or barrier reefs are identified in the Farsund Basin,

unlike in other examples (Rosleff-Soerensen et al. 2012; Saqab & Bourget 2016), although such features may be situated outside of the 3D seismic volume. Alternatively, the reefs within the Farsund Basin may be located in a natural sheltered environment.

5.4 Egersund and Tau formations – Deposition of anoxic shales

The Sandnes Formation is overlain by the Upper Jurassic Egersund and Tau Formations (Figure 3, 5). As determined from boreholes regionally, including well 11/5-1 in the Farsund Basin, these formations typically comprise organic-rich shales (Figure 5). Within the Farsund Basin, the Tau Formation has a slightly elevated Gamma Ray value (c. 120 API) when compared to the underlying Egersund Formation (c. 110 API) (Figure 5). Both formations are associated with a poorly reflective seismic facies within the basin (Figure 3, 5). Based on the observations outlined above, we interpret that the deposition of both the Egersund and Tau formations occurred in a low-energy environment, with the presence of pyritic and glauconitic horizons suggesting periodic anoxic conditions (Figure 5). Such an environment may indicate a sea level rise and marine transgression since the deposition of the Sandnes Formation, with deposition occurring in a deep marine environment, or may alternatively indicate deposition within a restricted, low-energy shallow-water environment (Van Der Zwaan & Jorissen 1991).

5.5 Sauda Formation - Delta progradation

A package of high-amplitude reflections is present at the top of the Jurassic interval, corresponding to the Sauda Formation in well 11/5-1 (Figure 3, 11). This reflection package is c. 40 ms TWT (c. 50 m) thick, thins southwards, and is associated with lateral changes in amplitude and low-angle clinoform sequences that downlap towards the south (Figure 11). These downlap terminations often correspond to the areas of amplitude brightening (Figure

11). The top and base of the high amplitude reflection package was mapped throughout the 3D volume, along with individual internal horizons. Seismic attributes were extracted from between these top and base horizons (Figure 11).

RMS amplitude, spectral decomposition and dip azimuth seismic attributes highlight a series of divergent, curvi-linear lineations in plan-view, defining high- and low-amplitude packages of varying frequency (Figure 12). Each band is c. 400 m wide, diverges westwards and displays a concave-to-south planform geometry. The bands are arranged into a series of discordant sets and thus truncate each other, at either low (i.e. Sets 1-3 in Figure 12d) or high angles (i.e. Set 4 in Figure 12d). Additional internal sets and truncations may tentatively be present, although these are not clear and accurately delineated within the data (Figure 12). The lineations are ubiquitous across the whole of the study area apart from across the footwall of the present-day Fjerritslev South Fault, where the Sauda Formation is absent due to erosion across the footwall of the fault (Figure 2, 12). The lineations are seemingly unaffected by the Fjerritslev North Fault, which cross-cuts but does not noticeably offset the lineations (Figure 12). Both the Fjerritslev North and Fjerritslev South Faults were not present at this time, becoming active in post-Sauda times. A set of N-S striking lineations (Set 4) are present to the northwest of the area and appear to correspond to the footwall of NS1, which was inactive at this time (Set 4; Figure 12). These lineations are concave to the east and diverge to the southwest. These N-S striking lineations also appear unaffected by the Fjerritslev North Fault, although they align with and are located along the footwall of NS1, suggesting this Triassic fault may have had some topographic expression at this time (Figure 12d). Faint lineations are identifiable in the southeast (Figure 12); these lineations are not associated with the Sauda Formation, which thins northwest of the area, but instead are related to subcrops of truncated underlying strata associated with salt mobilisation in this area. In some instances there appear to be mutual cross-cutting relationships between

individual sets of lineations (i.e. Set 2 and Set 4 in Figure 12d), rather than truncations against one another. However, these cross-cutting relationships are most likely due to signal mixing within the attribute extraction window; i.e. closely superposed sets produce cross-cutting relationships meaning their relative age cannot be distinguished in plan-view (Figure 12). The prominent lineations observed in plan-view (Figure 12) appear to correspond to the downlap terminations of clinoform sequences, or where the clinoform sequences thin below seismic resolution in cross-section (Figure 11).

Discordant sets of high-amplitude lineations identified in seismic reflection data, superficially similar to those observed here, have previously been interpreted as ancient shoreface beach ridge environments (Jackson et al. 2010; Klausen et al. 2015; Klausen et al. 2016). Such beach ridge systems typically comprise sand-rich ridges separated by elongate, typically lower energy, depressions (Otvos 2000), and form cuspate, concave-to-coastline morphologies comprising multiple discordant sets, formed through longshore drift (Billy et al. 2014; Vespremeanu-Stroe et al. 2016). Although geometrically similar, based on the lines of evidence outlined below we discount a beach-ridge origin for the lineations within the Farsund Basin. Firstly, the amplitude changes associated with the upper Jurassic curvi-linear features within the Farsund Basin are located downdip, or below the small-scale clinoform sequences (Figure 11), rather than being associated with the topsets as would be expected with a beach ridge interpretation (e.g. Jackson et al. 2010; Billy et al. 2014). Instead, the observed amplitude brightening may represent the tuned seismic response of the breakpoint (Dreyer et al. 2005) or down-dip terminations of the clinoforms themselves (Eide et al. 2017). Secondly, the concave-to-south planform geometries of the lineations would suggest that the paleo-shoreline was north-facing, an interpretation largely incompatible with the regional setting of the basin during the Late Jurassic, which was open to the south (Figure 1, 12). An additional and final argument against a beach ridge origin for these lineations lies in their

regional context. Using regional 2D seismic data, the high-amplitude lineations can be traced outside of the 3D volume. Here, they correspond to the lateral terminations of larger, lobate, high-amplitude packages that thicken northwards (Figure 13, 14). Overall, these packages are retrogradationally stacked, with clinoforms in younger packages downlapping onto the tops of older, underlying clinoform packages (Figure 13), causing the overall thickness of the Sauda Formation to increase northwards. This retrogradational stacking patterns suggests deposition during a period of relative sea level rise, at a time when the rate of accommodation generation outpaced sediment accumulation rates.

Individual clinoform-bearing packages are also partitioned laterally, forming a series of discrete lobes that are identified via concordant lineations and terminal downlapping reflections around their margins. The lateral terminations are also associated with an increase in amplitude as the package thins below seismic resolution and, we suggest, constructively tune (Figure 14). Based on these terminations we identify four main lobes, with the easternmost margin of the eastern lobe defined by an area of amplitude brightening (Figure 14).

The lobes forms an arcuate geometry in plan-view (Figure 15). Individual lobes prograde southwards, are c. 100 ms TWT (c. 140 m) thick and are 20-40 km wide (Figure 14, 15). They continue northwards into the Varnes Graben, which may represent a sediment fairway from the mainland (Figure 13), although a lack of data coverage in this area means their geometry cannot be constrained. As with the lineations identified in the 3D volume (Figure 12), individual lobes identified on the 2D data display discordant relationships with one another as younger lobes overlap and stack above and adjacent to older lobes (Figure 14, 15). The central lobe (Lobe 3) corresponds to the major lineations observed within the 3D volume (Sets 1 and 2; Figure 12). This lobe is situated at shallower stratigraphic levels and appears to overlap Lobe 2 situated to the east (Figure 15). Set 3 within the 3D volume may

also represent an older, stratigraphically deeper lobe (Lobe 1; Figure 15) that has been covered by lineation sets 1 and 2 of Lobe 3 (Figure 12, 15). Lobe 3 appears to be overlain by Lobe 4 to the west, which incorporates the lineations observed along the footwall of NS1 (Set 4, Figure 12d), as the thickness of the Upper Jurassic Sauda Formation increases westwards (Figure 14). This thickness change is representative of increased lobe stacking to the north and west (Figure 13, 15). We suggest that clinoform downlap terminations within individual lobes may give rise to the lineation sets observed in the 3D data (Figure 12). Furthermore, the overprinting and vertical stacking of different lobes may give rise to the discordant truncations of the lineation sets observed in the 3D data (Figure 12), with older lobes being partially overlapped by younger ones (Figure 15).

Based on this regional information, and in conjunction with the evidence outlined previously, we interpret that the lineations within the Upper Jurassic Sauda Formation correspond to the downlap termination of clinoforms within a series of deltaic lobes. The lobes prograded into an unconfined basin setting, with lobe avulsion causing them to stack laterally and vertically (Bridge & Leeder 1979; Jones & Schumm 1999). This interpretation is based on: i) the lobate geometry of the individual sequences (Figure 14, 15); ii) lateral downlap terminations at the margins of individual lobes (Figure 13, 15); iii) small-scale clinoforms indicative of deposition within a relatively shallow-water environment (Patruno et al. 2015a; Eide et al. 2017) (Figure 11, 13); iv) retrogradational stacking of individual lobes indicating the generation of accommodation outpaced sediment accumulation rate, potentially during a period of relative sea level rise (Figure 13); and v) progressive landward onlap of the Sauda Formation by Lower Cretaceous strata (Figure 13, 14). The Sauda Formation overlies the Egersund and Tau formations (Figure 5), which were deposited within an anoxic environment. A corollary of the interpretation here is that these anoxic shales were likely deposited within a shallow marine environment (Van Der Zwaan & Jorissen 1991), rather

than in deep-water, as the latter would require a drastic shallowing between the deposition of the two formations.

6 Discussion

Our model for the geomorphological evolution of the Farsund Basin, and our interpretations of the different facies types present (Figure 16), differs drastically from regional tectono-stratigraphic models of the area (Figure 1b) (Johannessen & Andsbjerg 1993; Andsbjerg 2003; Mannie et al. 2014; Mannie et al. 2016). Here, we first compare and contrast our model for the geomorphological evolution of the Farsund Basin outlined above to that more regionally, before discussing the implications for the structural evolution of the basin and regional tectonic activity, and the viability of petroleum systems in the area.

6.1 Regional paleo-geographical setting

The North Sea represented a predominately non-marine environment during the Permian, as recorded by deposition of the Rotliegend Group (Glennie 1997; van Wees et al. 2000; Glennie et al. 2003). Deposition of Zechstein salt in the Upper Permian occurred during a marine transgression and basin flooding (Glennie 1997; Glennie et al. 2003). East of the Farsund Basin, Jackson & Lewis (2013) define the depositional limit of mobile Zechstein salt striking ESE across the Lista Nose Fault Blocks (Figure 1). We find that this limit continues eastwards along-strike across the southern margin of the Farsund Basin, and did not extend north as far as previously described (Heeremans et al. 2004) (Figure 1). The local occurrence of small-scale, likely fluvio-deltaic, clinoforms (Patruno et al. 2015a) (Figure 6), and the non-marine Smith Bank and Skagerrak formations regionally (e.g. Goldsmith et al. 1995; McKie & Williams 2009; Jarsve et al. 2014), indicates a return to a sub-aerial environment during the Triassic. The Triassic clinoforms were likely sourced from mainland

Scandinavia to the north, and likely prograded southwards through the Varnes Graben (Figure 1).

Following Early-Mid Jurassic uplift, erosion and eventual deflation associated with the Mid North Sea thermal dome (Underhill & Partington 1993), the first formation to be preserved regionally was the Middle Jurassic Bryne Formation. This formation is encountered in the Egersund Basin, Norwegian-Danish Basin and the Danish Central Graben, where it consists of stacked fluvial and floodplain deposits deposited in a coastal-plain environment (Sørensen et al. 1992; Johannessen & Andsbjerg 1993; Andsbjerg 2003; Michelsen et al. 2003; Mannie et al. 2014; Mannie et al. 2016). Within the Farsund Basin, the Bryne Formation is represented by two E-trending channels deposited within a fluvio-deltaic environment (Figure 8e). At a regional scale the E-W orientation of these channels may be influenced by the Mid Jurassic thermal dome (Underhill & Partington 1993), flowing away from the site of maximum uplift. Alternatively, and in the authors view more likely, channel orientation may be controlled by more local uplift related to the Lista Nose Fault Blocks and Stavanger Platform to the west (Figure 1).

The Middle-Upper Jurassic (Callovian) Sandnes Formation documents a basinwide marine transgression, transitioning from a sub-aerial to shallow marine depositional environment, as observed elsewhere within the North Sea (Michelsen et al. 2003; Mannie et al. 2014; Mannie et al. 2016). This transgression was driven by a eustatic sea-level rise (Vail & Todd 1981; Sørensen et al. 1992), and may have been further augmented by rift-related thermal subsidence relating to a Permian-Triassic rift phase (Ziegler 1992). Within the Farsund Basin, the Sandnes Formation is manifest as a series of carbonate patch reefs (Figure 10), whereas elsewhere, including in the adjacent Egersund Basin, it contains only siliciclastic sediments (Figure 1b, 16) (e.g. Sørensen et al. 1992; Mannie et al. 2014; Mannie et al. 2016). The formation of carbonate patch reefs requires a lack of clastic sedimentation

546 within a relatively sediment starved basin. The lack of sediment within the Farsund Basin at
547 this time, compared to the Egersund Basin (Mannie et al. 2014; Mannie et al. 2016) may
548 reflect differences in their respective onshore source areas, and suggests that they were not
549 linked at this time.

550 In the Egersund Basin, facies shallow eastwards, from a fully marine environment to
551 a shoreface setting along the margin of the Stavanger Platform (Mannie et al. 2014). A
552 similar water depth change occurs within the Farsund Basin, although still largely within a
553 shallow-marine domain. Geomorphological features suggest relatively deeper water depths in
554 the east, represented by taller and, we infer, deeper-water patch reefs (Figure 9, 10, 16), and a
555 relatively shallow water depth towards the west which resulted in a dominance of shorter and
556 wider patch reefs. These complementary east- and west-facing shorefaces, and their
557 associated distinct facies belts (i.e. carbonate in the east and siliciclastic in the west) indicate
558 a relative high between the Egersund and Farsund Basins, potentially represented by
559 Stavanger Platform and Lista Nose Fault Blocks (Hamar et al. 1983; Sørensen et al. 1992).
560 One such topographic high, the Eigerøy Horst, continues northwards, as a series of
561 bathymetric highs termed the Hidra Mountains, to the Norwegian mainland where it may
562 reflect an onshore drainage divide (Rise et al. 2008).

563 Further relative sea-level increase is recorded by the deposition of the anoxic shales of
564 the Egersund and Tau formations (Vollset & Doré 1984; Sørensen et al. 1992). Cessation of
565 carbonate patch reef growth may have occurred due to a basin-wide transgression, or the
566 added input of the anoxic shales (Figure 16). Fine grained siltstones and claystones
567 comprising the Sauda Formation were deposited during the Upper Jurassic (Vollset & Doré
568 1984; Mannie et al. 2014), with a series of southwards-prograding and avulsing deltaic lobes
569 identified within the Farsund Basin (Figure 15, 16). This deltaic system has an extra-basinal
570 source, likely the Norwegian mainland, and was transported through the Carboniferous-

Permian-aged Varnes Graben, a sediment pathway during the Triassic (Heeremans et al. 2004; Jarsve et al. 2014). Lobe 4 however, may have a local sediment source, related to degradation of the Eigerøy Horst, which in this area forms the footwall of the Farsund North Fault (Figure 15). As with the stratigraphically older patch reefs, the deltaic lobes are also restricted westwards of, and are not present on, the Stavanger Platform (Figure 17).

West of the Stavanger Platform, additional deltaic sequences, the Hardangerfjord and Sognefjord units, are present within the Sauda Formation, sourced from and draining western Norway (Dreyer et al. 2005; Somme et al. 2013; Patruno et al. 2015b) (Figure 17). Wells penetrating the proximal part of the Hardangerfjord unit penetrate a mudstone dominated unit (Somme et al. 2013), whereas the Sognefjord unit has been shown to be more sandstone dominated (Patruno et al. 2015b). Within the Farsund Basin, well 11/5-1 penetrates a silty sandstone/sandstone interval corresponding to the distal part of the delta sequence; furthermore, the surrounding sediments are largely dominated by mudstones and siltstones (Figure 5), so a more sandstone-rich interval would produce the observed large impedance contrast (Figure 11, 13).

The partitioning between the Farsund deltaic sequence described here, and the Hardangerfjord unit located west of the Stavanger Platform appear to reflect the location of the drainage divide onshore Norway (Figure 17). Sediments sourced from west of the divide are deposited into the Hardangerfjord unit (Somme et al. 2013), and those east of the divide being deposited into the Farsund Basin and Skagerrak Sea (Somme et al. 2013; Jarsve et al. 2014) (Figure 17). The offshore continuation of this divide may be represented by the highs of the Eigerøy Horst, Stavanger Platform and Lista Nose Fault Blocks (Hamar et al. 1983; Skjerven et al. 1983) (Figure 17).

We have shown that the Farsund Basin contains different facies associations and experienced a markedly different tectono-stratigraphic evolution to basins to the west, separated by the Stavanger Platform and Lista Nose Fault Blocks. This may correspond to a boundary between different structural domains, between Caledonian Orogeny and post-orogenic collapse-dominated tectonics to the west (Phillips et al. 2016), and an evolution dominated by the Sorgenfrei-Tornquist Zone and the Tornquist trend to the east (Mogensen & Jensen 1994; Thybo 2000; Mogensen & Korstgård 2003; Phillips et al. 2018) (Figure 17).

6.2 Implications for tectonic activity

The Mesozoic structural evolution of this area is relatively understudied (Jensen & Schmidt 1993; Phillips et al. 2018). Here we use inferences from our proposed geomorphological evolution of the Farsund Basin to place additional constraints on its tectono-stratigraphic evolution along with more regional tectonics.

The depositional limit of the Zechstein salt reflects relative structural highs present at the time of deposition (Figure 1). Onlapping of the salt onto the southern margin of the Farsund Basin indicates that, at that time, the area to the north formed part of the Stavanger Platform, prior to later activity along the Fjerritslev North and South faults. This is in agreement with structural observations that the Farsund Basin did not exist in its present form until the Early Cretaceous (see Phillips et al. 2018). An abrupt step of c. 7 km is observed in the limit across NS2 (Figure 1). This step may reflect pre-existing topography within the basin at the time of deposition, post-depositional modification and translation of the boundary due to later fault activity, or a combination of both. NS2, along with other N-S striking faults may have been active during the Carboniferous-Permian extensional event (Heeremans & Faleide 2004; Heeremans et al. 2004), although due to a lack of imaging at depth within our seismic data, we are unable to confirm this. Pre-existing fault-related relief could cause such

a step in the depositional limit of mobile salt (Clark et al. 1998); similar steps are observed along-strike relating to the Stavanger Fault system (Figure 1) (Jackson & Lewis 2013). Additionally, the limit of the salt basin may have been modified post-deposition, perhaps relating to Early Jurassic sinistral strike-slip activity (Phillips et al. 2018).

East-trending fluvial channels within the Bryne Formation were, at least in part, controlled by the presence of thin-skinned, salt detached faults. A key observation is that these E-trending channels are not influenced by the major E-W striking faults, in particular the Fjerritslev South Fault, that delineate the present-day morphology of the basin. This concurs with structural observations, i.e. the lack of syn-kinematic pre-Cretaceous strata (Figure 3, 6), that the E-W faults were not active and had no surface expression at this time. The widening of fluvial channels across NS2 occurs across a subtle topographic gradient, interpreted as the paleo-shoreline. This topographic gradient may be related to differential compaction of underlying Triassic strata across NS2.

East-trending structures also have negligible influence on the formation and morphology of features within the Sandnes Formation. Patch reef morphology is unchanged across the E-W striking Fjerritslev North and South Faults, indicating that they grew in similarly shallow water depths (Figure 10) (Kendall & Schlager 1981). Conversely, patch reef morphology changes markedly across N-S striking faults, from short, wide reefs on the footwall, to tall, narrow reefs on the hangingwall (Figure 9, 10). Water depth has previously been shown to be a key factor in determining carbonate facies and patch reef morphology, with shallower water depths associated with shorter, wider reef morphologies (Brock et al. 2008), and favouring the formation of patch reefs over more continuous ridges (Colpaert et al. 2007; Purkis et al. 2015). Thus, we infer this change in reef morphology represents a change in water depth associated with the aforementioned topographic gradient across NS2 (Figure 9). Those patch reefs that grow in the slightly deeper water environment, i.e. the

hangingwall of NS2, exhibit catch-up growth as they attempt to reach shallower depths, forming tall, narrow structures (Kendall & Schlager 1981; Schlager 1981; Saqab & Bourget 2016). On the other hand, the wider patch reefs situated at shallow water level, i.e. the footwall of NS2, have no requirement for this catch-up growth and undergo keep-up growth, preferentially growing laterally, forming shorter, wider structures (Brock et al. 2008; Saqab & Bourget 2016). The occurrence of this catch-up/keep-up growth mechanism indicates that the growth of these structures was sensitive to water depth, and therefore that they formed as tropical carbonate reefs, as opposed to cool-water carbonates or carbonate mud mounds (Schlager 2000). Late Jurassic ocean temperatures were relatively equilibrated across the Tethyan Ocean, allowing tropical reefs to form across a large latitude range, including the Farsund Basin (Leinfelder 1994).

Following the deposition of the Egersund and Tau formations, a series of southwards prograding deltaic lobes were deposited in the Farsund Basin, forming part of the Upper Jurassic Sauda Formation. Lobe geometry appears unaffected by any underlying relief, with the Fjerritslev North and South faults now cross-cutting lobes. As they are now offset, this implies that no fault-related topography was present at the time of deposition and that the lobes were deposited in a relatively unconfined setting (Somme et al. 2013; Zhang et al. 2016). The lack of Upper Jurassic deltaic systems across the footwall of the Fjerritslev South Fault may be due to erosion following post-depositional fault activity and sub-aerial exposure of the footwall. Based on this, we infer that activity along the E-W Fjerritslev North and South faults in the Farsund Basin began in the Early Cretaceous, following the deposition of the deltaic system. Conversely, fault activity within the Egersund Basin started earlier, in the latest Jurassic, affecting the thickness and distribution of different facies (Mannie et al. 2014; Mannie et al. 2016). In the Farsund Basin, this likely corresponds to the same extensional event, with the age of the deltaic system straddling the Jurassic/Cretaceous boundary.

669 The Sauda Formation represents an input of sandstone deposited during an overall net
670 marine transgression (Mannie et al. 2016). This input of clastic material, both in the Farsund
671 Basin and offshore west Norway (Somme et al. 2013), corresponded to the late pre-rift to
672 peak-syn-rift stage of Late Jurassic-Early Cretaceous extension (Brun & Tron 1993; Bell et
673 al. 2014). The Early Cretaceous succession within the Farsund Basin predominately consists
674 of relatively deep marine sediments. Deposition of these sediments was associated with a
675 deepening of the Farsund Basin relating to Early Cretaceous tectonic activity (Mogensen &
676 Jensen 1994). This likely represents the same regional rift event documented to the west,
677 responsible for the deposition of the Hardangerfjord Delta sequence, although this event may
678 be regionally diachronous (Somme et al. 2013; Mannie et al. 2016).

679 **6.3 Implications for petroleum systems development of the Farsund Basin**
680

681 In constraining the geomorphological evolution of the Farsund Basin, we have also
682 identified a series of potential carbonate and clastic reservoirs that may form part of viable
683 petroleum systems. Channels identified within the Bryne Formation (Figure 7) are likely
684 composed of fluvial sandstones (Ryseth et al. 1998). In addition, carbonates, including patch
685 reefs such as those identified within the Sandnes Formation (Figure 9, 10), and offshore
686 deltaic systems akin to those within the Sauda Formation (Figure 11, 12, 15) have previously
687 been shown to represent viable petroleum reservoirs (Montgomery 1996; Moore 2001; Saller
688 et al. 2008).

689 The reservoir potential of the Sandnes Formation patch reefs is complicated due to
690 distinguishing between primary and secondary porosity within the reefs themselves (Enos &
691 Sawatsky 1981). Original porosity within carbonates can be enhanced through dissolution of
692 the host material, or alternatively, may be destroyed and infilled by secondary cementation.
693 This secondary porosity is dependent on a number of different factors. Typically, patch reefs

consist of a cemented core containing negligible porosity, with a less cemented, more porous surrounding framework (Enos & Sawatsky 1981). The high amplitude core and lower amplitude rim of the carbonate patch reefs as imaged in seismic data (Figure 9, 10a) may potentially reflect such a change in the degree of cementation, from a relatively compacted and cemented core, to a more porous rim. These complications notwithstanding, working patch reef plays have been discovered, such as the Lime Valley Pinnacle Reef Play, in Texas, USA (e.g. Montgomery 1996).

Stratigraphic and structural traps and seals are present within the Farsund Basin. The Zechstein salt would act as a regional seal throughout large parts of the area. However, areas to the north of the depositional limit of the salt may allow vertical migration into the Jurassic section (Figure 1). The carbonate patch reefs and fluvial channel systems are largely overlain by and encased in shales of the Egersund and Tau formations (Figure 3, 5). In addition, the isolated nature of the fluvial systems and the patch reefs allow them to represent discrete volumes. The lateral terminations of the Upper Jurassic deltaic lobes would also be expected to have s stratigraphic traps at their margins and are sealed by overlying Lower Cretaceous claystones and siltstones. Variable reservoir may be expected within the deltaic lobes; sandier material would be expected in the topsets and foresets of the clinoforms compared to the bottomsets, with a potential reduction in reservoir quality also expected around the distal margins of the lobes (Patruno et al. 2015a; Patruno et al. 2015b). Due to the main period of faulting along the E-W faults occurring following the deposition of the Jurassic interval, including these potential reservoir units (Figure 3, 6), a number of structural traps may also be present. Early Cretaceous faulting offsets and partitions the Upper Jurassic deltaic system into a series of discrete potential reservoir units (Figure 16).

In addition to these reservoirs, a number of potential source rocks are present throughout the area, each of varying maturity and likelihood of viability. The organic-rich

shales of the Tau Formation may be oil-mature in the centre of the Farsund Basin (Skjerven et al. 1983; Sørensen & Tangen 1995; Petersen et al. 2008). These correspond regionally to the Kimmeridge Clay and Draupne shales in the UK and Norwegian North Sea, respectively, which represent key source rock intervals in each area. The Tau Formation shales may be able to act as a local source rock for the identified Jurassic reservoirs. Regionally, the Cambrian aged Alum shales, situated to the east of the area (Petersen et al. 2008), may be mature and could act as a potential source rock in this region, although potential migration pathways into the Jurassic interval in this area seem far-fetched. Through constraining its geomorphological evolution we have identified and mapped key components of the petroleum system within the Farsund Basin, and have shown how seismic attribute driven interpretation can aid the imaging and mapping of petroleum systems in frontier areas.

7 Conclusions

In this study we have used a seismic attribute-driven approach to determine the geomorphological evolution of the Triassic-Jurassic succession in the Farsund Basin, offshore south Norway. Having established this local evolution, we link this to the tectono-stratigraphic evolution of the wider area and assess the viability of any potential petroleum systems. Overall, we find that:

1. The depositional limit of mobile Zechstein salt trends E-W across the southern margin of the Farsund Basin, onlapping the edge of the Stavanger Platform at the time of its deposition. A step in the depositional limit likely reflects base-salt relief relating to a pre-existing fault scarp, but may also be a result of post-depositional modification of the basin.
2. The geomorphological evolution of the Farsund Basin reflects an overall marine transgression, documented through the identification of fluvial river systems of the

Middle Jurassic Bryne Formation, shallow marine patch reefs developed within the Sandnes Formation, and Late Jurassic delta lobes within the Sauda Formation.

3. The morphology of the identified geomorphological features offer insights into the paleo-geographical setting of the basin. Paleo-topography, formed as a result of differential compaction across previously active faults, represents the paleo-shoreline and reflects a change in water depth throughout the deposition of the Bryne and Sandnes formations. The Upper Jurassic deltaic systems are unaffected by, and were therefore deposited prior to, the onset of faulting within the Farsund Basin
4. The tectono-stratigraphic evolution of the Farsund Basin differs markedly to that of the Egersund Basin to the west, due to the presence of a partition between the two areas. This partition is formed of structural highs corresponding to the Stavanger Platform and Lista Nose Fault Blocks offshore, and potentially the drainage divide onshore. These differing tectono-stratigraphic evolutions between the two areas reflects a difference in their regional tectonic settings, the evolution of the Egersund Basin area is controlled by Caledonian orogeny and orogenic collapse related structures, and the Farsund Basin by the underlying Sorgenfrei-Tornquist Zone.
5. Through this seismic geomorphological analysis we have identified a series of potential reservoirs, including fluvial systems, carbonate patch reefs, and offshore deltaic lobes, which along with seals and local sources within the Tau Formation, may form parts of working petroleum systems within the area.

This study showcases how seismic attributes and seismic geomorphological analysis can be used to determine the tectono-stratigraphic evolution of rift basins. These techniques are able to identify potential petroleum systems, representing a vital tool for the exploration of relatively underexplored frontier basins, and also offer insights into the structural evolution and wider tectonic settings of relatively underexplored basins.

Acknowledgements

This contribution forms part of the MultiRift project, funded by the Research Council of Norway's PETROMAKS programme (project number 215591) and Statoil to the University of Bergen and partners Imperial College, University of Manchester and University of Oslo. We thank the editor, Philip Ringrose, along with Bonita Barrett-Crosdil and an anonymous reviewer for their detailed reviews that greatly improved the quality of the manuscript. We also would like to thank PGS for allowing us to show and use the seismic data presented in this study and GeoTeric for providing us with academic licences for the software to undertake the spectral decomposition in the project. We would also like to thank Schlumberger for providing academic licences of the Petrel software to Imperial College.

Appendix A – Seismic attributes

Seismic attribute analysis was used to gain more information about the facies present across different stratigraphic levels within the Farsund Basin. RMS amplitude, variance, amplitude contrast, and spectral decomposition were calculated along a series of key stratigraphic horizons, with the attributes calculated across a window bounding the interval of interest specified in the text.

Root mean squared (RMS) amplitude is a measure of the absolute strength of the reflection, regardless of its polarity; stronger, brighter reflections are represented by higher RMS amplitude values.

Variance represents a measure of discordance between individual traces within the seismic data. The larger the difference between adjacent traces, the higher the variance value; therefore, this seismic attribute typically highlights the edges of discrete structures.

Amplitude contrast works in a similar way to the variance attribute, quantifying the lateral contrast in amplitude between adjacent traces.

Dip azimuth quantifies the dip magnitude and dip direction of the reflections, with the azimuth represented by a colour within a spectrum, and the dip by the shade of the colour. This attribute is calculated for each voxel within the data.

In addition to amplitude-derived attributes, we also investigated a number of frequency-derived attributes, to further interrogate the seismic reflection data. The frequency of the data with depth is shown in Figure 4, with an average frequency within the Jurassic interval of c. 35 Hz. Frequency is inherently linked to unit thickness, higher frequency values are able to resolve thinner units (Slatt 2006; Brown 2011).

Dominant frequency is a measure of frequency that accounts for both the instantaneous bandwidth and frequency, representing a relatively smoothed frequency value.

Spectral decomposition represents a colour blend of discrete frequency values extracted from the frequency spectrum of the data. The frequency spectrum of the data (Figure 4) is partitioned into a series of bins (each 20 Hz wide) which correspond to a range of frequencies. We then assign three of these frequency values to red, green and blue, representing low, medium and high frequency values, respectively; the brightness of each colour represents the power that frequency component contributes, i.e. red colours indicate a preponderance of lower frequencies, whereas structures with a response from all three frequency windows are represented by white. In this study, we assign frequency values of 22, 30 and 45 Hz to red, green and blue colours to produce our RGB spectral decomposition colour blend.

Figure captions

Figure 1 - A) TWT structure map showing the acoustic basement (Base upper Permian/Zechstein salt) surface throughout the study area. Red circles represent wells throughout the area, note the high density of well coverage in the Egersund Basin compared to the Farsund Basin. Also shown are the location of the 3D seismic survey referred to in this study and the salt depositional limits proposed by Jackson and Lewis (2013), Heeremans et al. (2014) and this study. B) Jurassic stratigraphic column. Lithostratigraphy from Mannie et al. (2016), focused on well data from the Egersund Basin, is contrasted against seismic data around well 11/5-1, located within the Farsund Basin. Note the lack of Triassic and Middle-Lower Jurassic strata in well 11/5-1.

Figure 2 – TWT structure maps of key stratigraphic horizons within the 3D volume located over the southern margin of the Farsund Basin. See Figure 1a for location and Figure 1b for the stratigraphic ages of horizons. A) TWT structure map of the Top Jurassic surface, dominated by the E-W striking Fjerritslev North and Fjerritslev South Faults. Also present is the N-S striking NS2 fault. B) TWT structure map of the stratigraphically deeper Base Jurassic Unconformity. C) TWT structure map of the base Zechstein salt acoustic basement surface. This surface is dominated by a series of N-S and E-W striking faults.

Figure 3 – Uninterpreted and interpreted seismic sections across the study area showing the Triassic and Jurassic intervals. Note that the Jurassic interval appears restorable across the Fjerritslev South Fault, indicating that fault activity occurred later, during the Early Cretaceous. Also, the upper Jurassic interval appears eroded from the footwall of the Fjerritslev South Fault. Structures analysed in sections 5.1, 5.2, 5.3 and 5.5 are labelled on the interpreted section. See Figure 2 for location.

Figure 4 – A) Frequency vs depth throughout the Farsund Basin in the vicinity of the 11/5-1 well. Inset - closeup of the changing frequency with depth within the Jurassic interval. Frequency was calculated within a 3-point moving average. Vertical resolution was also calculated at various depths. B) Frequency spectrum for the 3D seismic volume. Also shown are the extracted frequency bins combined to create the spectral decomposition seismic attribute.

Figure 5 – Well log information and synthetic seismic for the Jurassic interval of well 11/5-1. Synthetic seismic section was created using the RHOB and DT wireline logs of the well. A lack of density data at around 1130-1180m results in a major discrepancy between the original and synthetic seismic data. Otherwise, the synthetic provides a good match to the original seismic at the Rotliegend Group and Sandnes Formation intervals, as well as the Sauda Formation.

Figure 6 – Uninterpreted and interpreted seismic section showing the northwards limit of thin-skinned, salt-detached faulting marking the northern depositional limit of mobile salt. Also note that an undeformed clinoform interval progrades southwards before being offset by thin-skinned faulting to the south. See Figure 2 for location.

Figure 7 – Uninterpreted and interpreted N-trending seismic sections across the southern margin of the Farsund Basin, see Figure 2 for location. Two distinct high-amplitude features can be observed at the base of the Jurassic interval corresponding to channel systems. Note that the channel systems are predominately situated within the hangingwalls of the thin-skinned, salt-detached faults.

Figure 8 – Seismic attribute maps of the southern margin of the Farsund Basin, calculated in a 25 ms TWT window below the top of the high amplitude structures. A) TWT structure map of the area, located at the intersection of the NS2 and Fjerritslev South faults. B) RMS amplitude seismic attribute, highlighting two high amplitude E-trending channel-like features, widening across NS2. C) Variance seismic attribute, further delineating the margins of the structures. D) Dominant frequency attribute, showing the overall geometry of the features and showing a decrease in frequency in the centre of the structure towards the east. E) Interpretation, based on the seismic attributes above, of these features as a fluvial channel system, widening into a more deltaic environment across NS2.

Figure 9 – Uninterpreted and interpreted seismic section showing a series of discrete high amplitude structures within the Sandnes Formation. A wider, shorter structure is present on the footwall of NS2, with taller, narrower structures on the hangingwall. See Figure 2 for location.

Figure 10 – Compilation of seismic attributes extracted from a 50 ms TWT window above the Base Jurassic Unconformity across the whole of the 3D seismic volume, see Figure 1 for location. A) RMS

amplitude highlighting high amplitude, sub-circular structures. B) Spectral decomposition, highlighting sub-circular structures, including those on the hangingwall of NS2. C) Variance, showing that the structures contain few internal discontinuities. D) Interpretation of the area, showing wider sub-circular structures, interpreted as carbonate patch reefs, on the footwall of NS2 and smaller structures on the hangingwall. E) Seismic section showing a composite reef, formed through the radial growth and coalescence of two individual reefs. See Figure 10d for location. F) Seismic section showing a reef offset by later faulting, implying a brittle nature. See Figure 10d for location.

Figure 11 – Uninterpreted and interpreted seismic section showing lateral amplitude changes within the upper Jurassic Sauda Formation. Two distinct sets can be identified (Set 2 and Set 3), defined by downlap terminations of clinoform structures. Grey arrow corresponds to the location marked by the grey arrow on Figure 12. See Figures 2 and 12 for location.

Figure 12 – Seismic attribute maps across the 3D seismic volume extracted from a window between the top and the base of the high amplitude package (see Figure 11). The white line indicates the location of Figure 11, whilst the grey arrow corresponds to that shown on Figure 11. A) RMS amplitude attribute map showing a series of concave to the south, curvilinear high amplitude lineations. B) Spectral decomposition seismic attribute, highlighting internal lineation geometries and relationships between individual sets. C) Dip azimuth of the lineations, further highlighting the curvilinear and discordant nature of the lineation sets. D) Interpretation of the lineation sets. The curvilinear lineations are arranged into a series of discordant sets that truncate each other at low angles. A further, concave-to-the-east lineation set is present along the footwall of NS1. Note that the lineations are not present across the footwall of the Fjerritslev South Fault and do not appear to be influenced by the Fjerritslev North Fault.

Figure 13 – Uninterpreted and interpreted N-S oriented regional 2D seismic section across the Farsund Basin. See Figure 1 for location. The area also imaged in the 3D volume is situated to the south. A series of deltaic systems are identified prograding southwards and aggrading and stacking atop one another, as evidenced by downlap terminations. The base of the Sauda Formation is marked as a reference horizon by a blue dashed line on the uninterpreted section.

Figure 14 – Uninterpreted and interpreted E-W oriented regional 2D seismic section. See Figure 1 for location. Three discrete deltaic lobes can be identified across the area, with lateral downlap terminations observed either side. These lobes appear to thicken towards the west. The base of the Sauda Formation is marked as a reference horizon by a blue dashed line on the uninterpreted section.

Figure 15 – Compilation and map-view geometry of individual lobes associated with the fan system in the Sauda Formation. The location of the 3D volume is shown by the black polygon whilst grey lines mark the major faults. Individual lineation sets as identified in Figure 12 are labelled in blue. Different structural elements are shown in various shades of grey. Fan geometries are based on lateral downlap terminations within the 2D data (see Figure 13 and 14), and the lineations identified within the 3D volume. A series of deltaic lobes are identified, prograding from the north and stacking progressively towards the west.

Figure 16 –Left. A) Coastal plain-shallow marine environment during the deposition of the Bryne Formation with eastwards flowing fluvial systems widening into a more deltaic environment across NS2. B) Patch reef development within a sheltered shallow marine environment during the deposition of the Sandnes Formation. Wide, short patch reefs present in shallower water pass eastwards into a deeper environment, consisting of tall, narrow patch reefs, across the NS2 fault. C) Progradation of shallow marine deltaic systems from the north during the Late Jurassic and the deposition of the Sauda Formation. Right – Tectono-stratigraphic chart showing the local evolution of the Farsund Basin as evidenced in this study. N-S striking faults, NS1 and NS2, were active during the Triassic, whereas E-W striking faults, i.e. the Fjerritslev North and South Faults, and the Farsund North Fault, were active during Early Cretaceous rifting.

Figure 17 – Regional tectono-stratigraphic setting of the study area during the Late Jurassic and deposition of the Sauda Formation. The Farsund Basin is dominated by the progradation of the Farsund Delta, whereas the Egersund Basin is dominated by the Hardangerfjord Delta, with the two areas separated by the intervening structural high of the Stavanger Platform and Lista Nose Fault Blocks.

References

Agirrezabala, L.M., Kiel, S., Blumenberg, M., Schäfer, N. & Reitner, J. 2013. Outcrop analogues of pockmarks and associated methane-seep carbonates: A case study from the Lower Cretaceous (Albian) of the Basque-Cantabrian Basin, western Pyrenees. *Palaeogeography, Palaeoclimatology, Palaeoecology*, **390**, 94-115, http://doi.org/http://dx.doi.org/10.1016/j.palaeo.2012.11.020.

Andresen, K.J., Huuse, M., Schodt, N.H., Clausen, L.F. & Seidler, L. 2011. Hydrocarbon plumbing systems of salt minibasins offshore Angola revealed by three-dimensional seismic analysis. *AAPG Bulletin*, **95**, 1039-1065.

Andsbjerg, J. 2003. Sedimentology and sequence stratigraphy of the Bryne and Lulu formations, middle Jurassic, northern Danish Central Graben. *The Jurassic of Denmark and Greenland. Geological Survey of Denmark and Greenland Bulletin*, **1**, 301-347.

Bell, R.E., Jackson, C.A.L., Whipp, P.S. & Clements, B. 2014. Strain migration during multiphase extension: Observations from the northern North Sea. *Tectonics*, **33**, 1936-1963, http://doi.org/10.1002/2014TC003551.

Billy, J., Robin, N., Hein, C.J., Certain, R. & FitzGerald, D.M. 2014. Internal architecture of mixed sand-and-gravel beach ridges: Miquelon-Langlade Barrier, NW Atlantic. *Marine Geology*, **357**, 53-71, http://doi.org/http://dx.doi.org/10.1016/j.margeo.2014.07.011.

Bridge, J.S. & Leeder, M.R. 1979. A simulation model of alluvial stratigraphy. *Sedimentology*, **26**, 617-644, http://doi.org/doi:10.1111/j.1365-3091.1979.tb00935.x.

Brock, J.C., Palaseanu-Lovejoy, M., Wright, C.W. & Nayegandhi, A. 2008. Patch-reef morphology as a proxy for Holocene sea-level variability, Northern Florida Keys, USA. *Coral Reefs*, **27**, 555-568.

Brown, A.R. 2011. *Interpretation of three-dimensional seismic data*. Society of Exploration Geophysicists and American Association of Petroleum Geologists.

Brun, J.-P. & Tron, V. 1993. Development of the North Viking Graben: inferences from laboratory modelling. *Sedimentary Geology*, **86**, 31-51.

Cartwright, J. & Huuse, M. 2005. 3D seismic technology: the geological 'Hubble'. *Basin Research*, **17**, 1-20, http://doi.org/10.1111/j.1365-2117.2005.00252.x.

Chopra, S. & Marfurt, K.J. 2008. Emerging and future trends in seismic attributes. *The Leading Edge*, **27**, 298-318, http://doi.org/10.1190/1.2896620.

Christensen, J.E. & Korstgård, J.A. 1994. The Fjerritslev Fault offshore Denmark - salt and fault interactions. *First Break*, **12**, 31-42, http://doi.org/10.3997/1365-2397.1994003

965 Clark, J.A., Stewart, S.A. & Cartwright, J.A. 1998. Evolution of the NW margin of the North Permian
966 Basin, UK North Sea. *Journal of the Geological Society*, **155**, 663-676, http://doi.org/DOI
967 10.1144/gsjgs.155.4.0663.

968
969 Colpaert, A., Pickard, N., Mienert, J., Henriksen, L.B., Rafaelsen, B. & Andreassen, K. 2007. 3D
970 seismic analysis of an Upper Palaeozoic carbonate succession of the Eastern Finnmark Platform area,
971 Norwegian Barents Sea. *Sedimentary Geology*, **197**, 79-98,
972 http://doi.org/http://dx.doi.org/10.1016/j.sedgeo.2006.09.001.

973
974 Coward, M.P., Dewey, J.F., Hempton, M. & Holroyd, J. 2003. Tectonic evolution. *In*: Evans, D.,
975 Graham, C., Armour, A. & Bathurst, P. (eds) *The Millenium Atlas: petroleum geology of the central*
976 *and northern North Sea*, Geological Society of London.

977
978 Davies, R.J. & Stewart, S.A. 2005. Emplacement of giant mud volcanoes in the South Caspian Basin:
979 3D seismic reflection imaging of their root zones. *Journal of the Geological Society*, **162**, 1-4,
980 http://doi.org/10.1144/0016-764904-082.

981
982 Dreyer, T., Whitaker, M., Dexter, J., Flesche, H. & Larsen, E. 2005. From spit system to tide-
983 dominated delta: integrated reservoir model of the Upper Jurassic Sognefjord Formation on the Troll
984 West Field. *Geological Society, London, Petroleum Geology Conference series*, **6**, 423-448,
985 http://doi.org/10.1144/0060423.

986
987 Eide, C.H., Klausen, T.G., Katkov, D., Suslova, A.A. & Helland-Hansen, W. 2017. Linking an Early
988 Triassic delta to antecedent topography: Source-to-sink study of the southwestern Barents Sea margin.
989 *GSA Bulletin*, **130**, 263-283, http://doi.org/10.1130/b31639.1.

990
991 Enos, P. & Sawatsky, L.H. 1981. Pore networks in Holocene carbonate sediments. *Journal of*
992 *Sedimentary Research*, **51**, 961-985, http://doi.org/10.1306/212f7df1-2b24-11d7-8648000102c1865d.

993
994 Færseth, R.B. 1996. Interaction of Permo-Triassic and Jurassic extensional fault-blocks during the
995 development of the northern North Sea. *Journal of the Geological Society*, **153**, 931-944,
996 http://doi.org/10.1144/gsjgs.153.6.0931.

997
998 Fichler, C., Henriksen, S., Rueslaatten, H. & Hovland, M. 2005. North Sea Quaternary morphology
999 from seismic and magnetic data:indications for gas hydrates during glaciation. *Petroleum Geoscience*,
1000 **11**, 331-337, http://doi.org/10.1144/1354-079304-635.

1001
1002 Glennie, K.W. 1997. Recent advances in understanding the southern North Sea Basin: a summary.
1003 *Geological Society, London, Special Publications*, **123**, 17-29,
1004 http://doi.org/10.1144/gsl.sp.1997.123.01.03.

1005
1006 Glennie, K.W., Higham, J. & Stemmerik, L. 2003. Permian. *In*: Evans, D. (ed) *The Millenium Atlas:*
1007 *Petroleum geology of the Central and Northern North Sea*. The Geological Society of London.

1008
1009 Goldsmith, P.J., Rich, B. & Standring, J. 1995. Triassic correlation and stratigraphy in the South
1010 Central Graben, UK North Sea. *Geological Society, London, Special Publications*, **91**, 123-143,
1011 http://doi.org/10.1144/gsl.sp.1995.091.01.07.

Hamar, G., Fjaeran, T. & Hesjedal, A. 1983. Jurassic stratigraphy and tectonics of the south-southeastern Norwegian offshore. *Petroleum Geology of the Southeastern North Sea and the Adjacent Onshore Areas*. Springer, 103-114.

Heeremans, M. & Faleide, J.I. 2004. Late Carboniferous-Permian tectonics and magmatic activity in the Skagerrak, Kattegat and the North Sea. *Geological Society, London, Special Publications*, **223**, 157-176.

Heeremans, M., Faleide, J.I. & Larsen, B.T. 2004. Late Carboniferous -Permian of NW Europe: an introduction to a new regional map. *Geol Soc London, Special Publication*, **223**, 75-88.

Holgate, N.E., Jackson, C.A.L., Hampson, G.J. & Dreyer, T. 2013. Sedimentology and sequence stratigraphy of the Middle–Upper Jurassic Krossfjord and Fensfjord formations, Troll Field, northern North Sea. *Petroleum Geoscience*, **19**, 237.

Holgate, N.E., Hampson, G.J., Jackson, C.A.-L. & Petersen, S.A. 2014. Constraining uncertainty in interpretation of seismically imaged clinoforms in deltaic reservoirs, Troll field, Norwegian North Sea: Insights from forward seismic models of outcrop analogs. *AAPG Bulletin*, **98**, 2629-2663.

Hovland, M., Talbot, M.R., Qvale, H., Olaussen, S. & Aasberg, L. 1987. Methane-Related Carbonate Cements in Pockmarks of the North-Sea. *Journal of Sedimentary Research*, **57**, 881-892.

Jackson, C.A.L. & Lewis, M.M. 2013. Physiography of the NE margin of the Permian Salt Basin: new insights from 3D seismic reflection data. *Journal of the Geological Society*, **170**, 857-860, http://doi.org/10.1144/jgs2013-026.

Jackson, C.A.L., Chua, S.T., Bell, R.E. & Magee, C. 2013. Structural style and early stage growth of inversion structures: 3D seismic insights from the Egersund Basin, offshore Norway. *Journal of Structural Geology*, **46**, 167-185, http://doi.org/http://dx.doi.org/10.1016/j.jsg.2012.09.005.

Jackson, C.A.L., Grunhagen, H., Howell, J.A., Larsen, A.L., Andersson, A., Boen, F. & Groth, A. 2010. 3D seismic imaging of lower delta-plain beach ridges: lower Brent Group, northern North Sea. *Journal of the Geological Society*, **167**, 1225-1236.

Jackson, M.P.A. & Talbot, C.J. 1986. External Shapes, Strain Rates, and Dynamics of Salt Structures. *Geological Society of America Bulletin*, **97**, 305-323, http://doi.org/Doi 10.1130/0016-7606(1986)97<305:Essrad>2.0.Co;2.

Jarsve, E.M., Maast, T.E., Gabrielsen, R.H., Faleide, J.I., Nystuen, J.P. & Sasier, C. 2014. Seismic stratigraphic subdivision of the Triassic succession in the Central North Sea; integrating seismic reflection and well data. *Journal of the Geological Society*, **171**, 353-374, http://doi.org/10.1144/jgs2013-056.

Jensen, L.N. & Schmidt, B.J. 1993. Neogene uplift and erosion offshore south Norway: magnitude and consequences for hydrocarbon exploration in the Farsund Basin. *In*: Spencer, A.M. (ed.) *Spec. Publ. European Association of Petroleum Geoscientists*. Springer.

Johannessen, P.N. & Andsbjerg, J. 1993. Middle to Late Jurassic basin evolution and sandstone reservoir distribution in the Danish Central Trough. *Geological Society, London, Petroleum Geology Conference 			series*, **4**, 271-283, http://doi.org/10.1144/0040271.

Jones, L. & Schumm, S. 1999. Causes of avulsion: an overview *Fluvial sedimentology VI*. Spec. Publ. Int. Assoc. Sedimentol, **28**, 171-178.

Kallweit, R.S. & Wood, L.C. 1982. The limits of resolution of zero-phase wavelets. *GEOPHYSICS*, **47**, 1035-1046, http://doi.org/10.1190/1.1441367.

Kendall, C.G.S.C. & Schlager, W. 1981. Carbonates and relative changes in sea level. *Marine Geology*, **44**, 181-212.

Klausen, T.G., Ryseth, A., Helland-Hansen, W. & Gjelberg, H.K. 2016. Progradational and backstepping shoreface deposits in the Ladinian to Early Norian Snadd Formation of the Barents Sea. *Sedimentology*, **63**, 893-916, http://doi.org/10.1111/sed.12242.

Klausen, T.G., Ryseth, A.E., Helland-Hansen, W., Gawthorpe, R. & Laursen, I. 2015. Regional development and sequence stratigraphy of the Middle to Late Triassic Snadd Formation, Norwegian Barents Sea. *Marine and Petroleum Geology*, **62**, 102-122, http://doi.org/http://dx.doi.org/10.1016/j.marpetgeo.2015.02.004.

Kluesner, J.W., Silver, E.A., Bangs, N.L., McIntosh, K.D., Gibson, J., Orange, D., Ranero, C.R. & von Huene, R. 2013. High density of structurally controlled, shallow to deep water fluid seep indicators imaged offshore Costa Rica. *Geochemistry, Geophysics, Geosystems*, **14**, 519-539, http://doi.org/10.1002/ggge.20058.

Legler, B., Hampson, G.J., Jackson, C.A., Johnson, H.D., Massart, B.Y., Sarginson, M. & Ravnås, R. 2014. Facies relationships and stratigraphic architecture of distal, mixed tide-and wave-influenced deltaic deposits: Lower Sego sandstone, western Colorado, USA. *Journal of Sedimentary Research*, **84**, 605-625.

Leinfelder, R.R. 1994. Distribution of Jurassic reef types: a mirror of structural and environmental changes during breakup of Pangea *Pangea: Global Environments and Resources*. CSPG Special Publications, AAPG Memoir, **17**, 677-700.

Lewis, M.M., Jackson, C.A.L. & Gawthorpe, R.L. 2013. Salt-influenced normal fault growth and forced folding: The Stavanger Fault System, North Sea. *Journal of Structural Geology*, **54**, 156-173, http://doi.org/10.1016/j.jsg.2013.07.015.

Magee, C., Duffy, O.B., Purnell, K., Bell, R.E., Jackson, C.A.L. & Reeve, M.T. 2016. Fault-controlled fluid flow inferred from hydrothermal vents imaged in 3D seismic reflection data, offshore NW Australia. *Basin Research*, **28**, 299-318, http://doi.org/10.1111/bre.12111.

Mannie, A.S., Jackson, C.A.L. & Hampson, G.J. 2014. Structural controls on the stratigraphic architecture of net-transgressive shallow-marine strata in a salt-influenced rift basin: Middle-to-Upper

Jurassic Egersund Basin, Norwegian North Sea. *Basin Research*, **26**, 675-700, http://doi.org/10.1111/bre.12058.

Mannie, A.S., Jackson, C.A.L., Hampson, G.J. & Fraser, A.J. 2016. Tectonic controls on the spatial distribution and stratigraphic architecture of a net-transgressive shallow-marine synrift succession in a salt-influenced rift basin: Middle to Upper Jurassic, Norwegian Central North Sea. *Journal of the Geological Society*, **173**, 901-915, http://doi.org/10.1144/jgs2016-033.

Marcon, Y., Ondréas, H., Sahling, H., Bohrmann, G. & Olu, K. 2014. Fluid flow regimes and growth of a giant pockmark. *Geology*, **42**, 63-66, http://doi.org/10.1130/g34801.1.

McKie, T. & Williams, B. 2009. Triassic palaeogeography and fluvial dispersal across the northwest European Basins. *Geological Journal*, **44**, 711-741, http://doi.org/10.1002/gj.1201.

Michelsen, O., Nielsen, L.H., Johannessen, P.N., Andsbjerg, J. & Surlyk, F. 2003. The Jurassic of Denmark and Greenland: Jurassic lithostratigraphy and stratigraphic development onshore and offshore Denmark.

Mogensen, T.E. & Jensen, L.N. 1994. Cretaceous subsidence and inversion along the Tornquist Zone from Kattegat to the Egersund Basin. *First Break*, **12**, 211-222.

Mogensen, T.E. & Korstgård, J.A. 2003. Triassic and Jurassic transtension along part of the Sorgenfrei-Tornquist Zone in the Danish Kattegat. *Geological Survey of Denmark and Greenland Bulletin*, **1**, 439-458.

Montgomery, S.L. 1996. Cotton Valley lime pinnacle reef play: Branton Field. *AAPG Bulletin*, **80**, 617-629.

Moore, C.H. 2001. *Carbonate reservoirs: porosity, evolution and diagenesis in a sequence stratigraphic framework*. Elsevier.

Nielsen, L.H. 2003. Late Triassic–Jurassic development of the Danish Basin and the Fennoscandian Border Zone, southern Scandinavia. *The Jurassic of Denmark and Greenland. Geological Survey of Denmark and Greenland Bulletin*, **1**, 459-526.

Olivarius, M. & Nielsen, L.H. 2016. Triassic paleogeography of the greater eastern Norwegian-Danish Basin: Constraints from provenance analysis of the Skagerrak Formation. *Marine and Petroleum Geology*, **69**, 168-182, http://doi.org/http://dx.doi.org/10.1016/j.marpetgeo.2015.10.008.

Otvos, E.G. 2000. Beach ridges—definitions and significance. *Geomorphology*, **32**, 83-108.

Patruno, S., Hampson, G.J. & Jackson, C.A.L. 2015a. Quantitative characterisation of deltaic and subaqueous clinoforms. *Earth-Science Reviews*, **142**, 79-119, http://doi.org/http://dx.doi.org/10.1016/j.earscirev.2015.01.004.

Patruno, S., Hampson, G.J., Jackson, C.A.L. & Dreyer, T. 2015b. Clinoform geometry, geomorphology, facies character and stratigraphic architecture of a sand-rich subaqueous delta: Jurassic Sognefjord Formation, offshore Norway. *Sedimentology*, **62**, 350-388, http://doi.org/10.1111/sed.12153.

Petersen, H., Nielsen, L., Bojesen-Koefoed, J.A., Mathiesen, A., Kristensen, L. & Dalhoff, F. 2008. Evaluation of the quality, thermal maturity and distribution of potential source rocks in the Danish part of the Norwegian–Danish Basin. *Geological Survey of Denmark and Greenland Bulletin*, **16**, 1-27.

Phillips, T.B., Jackson, C.A.L., Bell, R.E. & Duffy, O.B. 2018. Oblique reactivation of lithosphere-scale lineaments controls rift physiography – the upper-crustal expression of the Sorgenfrei–Tornquist Zone, offshore southern Norway. *Solid Earth*, **9**, 403-429, http://doi.org/10.5194/se-9-403-2018.

Phillips, T.B., Jackson, C.A.L., Bell, R.E., Duffy, O.B. & Fossen, H. 2016. Reactivation of intrabasement structures during rifting: A case study from offshore southern Norway. *Journal of Structural Geology*, **91**, 54-73, http://doi.org/http://dx.doi.org/10.1016/j.jsg.2016.08.008.

Posamentier, H. & Laurin, P. 2005. Seismic geomorphology of oligocene to miocene carbonate buildups offshore Madura, Indonesia *SEG Technical Program Expanded Abstracts 2005*. Society of Exploration Geophysicists, 429-431.

Posamentier, H.W. 2004. Seismic geomorphology: imaging elements of depositional systems from shelf to deep basin using 3D seismic data: implications for exploration and development. *Geological Society, London, Memoirs*, **29**, 11-24.

Posamentier, H.W. & Kolla, V. 2003. Seismic geomorphology and stratigraphy of depositional elements in deep-water settings. *Journal of Sedimentary Research*, **73**, 367-388.

Prélat, A., Hodgson, D.M. & Flint, S.S. 2009. Evolution, architecture and hierarchy of distributary deep-water deposits: a high-resolution outcrop investigation from the Permian Karoo Basin, South Africa. *Sedimentology*, **56**, 2132-2154, http://doi.org/10.1111/j.1365-3091.2009.01073.x.

Purkis, S., Casini, G., Hunt, D. & Colpaert, A. 2015. Morphometric patterns in Modern carbonate platforms can be applied to the ancient rock record: Similarities between Modern Alacranes Reef and Upper Palaeozoic platforms of the Barents Sea. *Sedimentary Geology*, **321**, 49-69, http://doi.org/http://dx.doi.org/10.1016/j.sedgeo.2015.03.001.

Rattey, R.P. & Hayward, A.B. 1993. Sequence Stratigraphy of a Failed Rift System - the Middle Jurassic to Early Cretaceous Basin Evolution of the Central and Northern North-Sea. *Petroleum Geology of Northwest Europe: Proceedings of the 4th Conference*, **4**, 215-249, http://doi.org/Doi 10.1144/0040215.

Rise, L., Bøe, R., Ottesen, D., Longva, O. & Olsen, H.A. 2008. Postglacial depositional environments and sedimentation rates in the Norwegian Channel off southern Norway. *Marine Geology*, **251**, 124-138, http://doi.org/https://doi.org/10.1016/j.margeo.2008.02.012.

Romans, B.W., Fildani, A., Hubbard, S.M., Covault, J.A., Fosdick, J.C. & Graham, S.A. 2011. Evolution of deep-water stratigraphic architecture, Magallanes Basin, Chile. *Marine and Petroleum Geology*, **28**, 612-628, http://doi.org/https://doi.org/10.1016/j.marpetgeo.2010.05.002.

Rosleff-Soerensen, B., Reuning, L., Back, S. & Kukla, P. 2012. Seismic geomorphology and growth architecture of a Miocene barrier reef, Browse Basin, NW-Australia. *Marine and Petroleum Geology*, **29**, 233-254, http://doi.org/https://doi.org/10.1016/j.marpetgeo.2010.11.001.

Ruf, A., Simo, J.A. & Hughes, T.M. 2008. Quantitative Characterization of Oligocene-Miocene Carbonate Mound Morphology from 3D Seismic Data: Applications to Geologic Modeling, East Java Basin, Indonesia. International Petroleum Technology Conference.

Ryseth, A., Fjellbirkeland, H., Osmundsen, I.K., Skålnes, Å. & Zachariassen, E. 1998. High-resolution stratigraphy and seismic attribute mapping of a fluvial reservoir: Middle Jurassic Ness Formation, Oseberg Field. *AAPG Bulletin*, **82**, 1627-1651.

Saller, A., Werner, K., Sugiaman, F., Cebastiant, A., May, R., Glenn, D. & Barker, C. 2008. Characteristics of Pleistocene deep-water fan lobes and their application to an upper Miocene reservoir model, offshore East Kalimantan, Indonesia. *AAPG Bulletin*, **92**, 919.

Saqab, M.M. & Bourget, J. 2016. Seismic geomorphology and evolution of early–mid Miocene isolated carbonate build-ups in the Timor Sea, North West Shelf of Australia. *Marine Geology*, **379**, 224-245, http://doi.org/http://dx.doi.org/10.1016/j.margeo.2016.06.007.

Schlager, W. 1981. The paradox of drowned reefs and carbonate platforms. *Geological Society of America Bulletin*, **92**, 197.

Schlager, W. 2000. Sedimentation rates and growth potential of tropical, cool-water and mud-mound carbonate systems. *Geological Society, London, Special Publications*, **178**, 217-227, http://doi.org/10.1144/gsl.sp.2000.178.01.14.

Skjerven, J., Rijs, F. & Kalheim, J. 1983. Late Palaeozoic to Early Cenozoic structural development of the south-southeastern Norwegian North Sea. *Petroleum Geology of the Southeastern North Sea and the Adjacent Onshore Areas*. Springer, 35-45.

Slatt, R.M. 2006. *Stratigraphic reservoir characterization for petroleum geologists, geophysicists, and engineers*. Elsevier.

Somme, T.O., Martinsen, O.J. & Lunt, I. 2013. Linking offshore stratigraphy to onshore paleotopography: The Late Jurassic-Paleocene evolution of the south Norwegian margin. *Geological Society of America Bulletin*, **125**, 1164-1186, http://doi.org/10.1130/b30747.1.

Sørensen, S. & Tangen, O.H. 1995. Exploration trends in marginal basins from Skagerrak to Stord. *In*: Hanslien, S. (ed) *Norwegian Petroleum Society Special Publications*. Elsevier, **Volume 4**, 97-114.

1243 Sørensen, S., Morizot, H. & Skottheim, S. 1992. A tectonostratigraphic analysis of the southeast
1244 Northern North Sea Basin. *In*: Larsen, R.M., Brekke, H., Larsen, B.T. & Talleraas, E. (eds) *Structural*
1245 *and Tectonic modelling and its application to Petroleum Geology*. Elsevier, Amsterdam, **1**, 19-42.

1246
1247 Stewart, S. 1999. Seismic interpretation of circular geological structures. *Petroleum Geoscience*, **5**,
1248 273-285.

1249
1250 Thybo, H. 2000. Crustal structure and tectonic evolution of the Tornquist Fan region as revealed by
1251 geophysical methods. *Bulletin of the Geological Society of Denmark*, **46**, 145-160.

1252
1253 Tvedt, A.B.M., Rotevatn, A., Jackson, C.A.L., Fossen, H. & Gawthorpe, R.L. 2013. Growth of
1254 normal faults in multilayer sequences: A 3D seismic case study from the Egersund Basin, Norwegian
1255 North Sea. *Journal of Structural Geology*, **55**, 1-20, http://doi.org/10.1016/j.jsg.2013.08.002.

1256
1257 Underhill, J.R. & Partington, M.A. 1993. Jurassic thermal doming and deflation in the North Sea:
1258 implications of the sequence stratigraphic evidence. 337-345, http://doi.org/10.1144/0040337.

1259
1260 Vail, P.R. & Todd, R.G. 1981. Northern North Sea Jurassic unconformities, chronostratigraphy and
1261 sea-level changes from seismic stratigraphy. *Petroleum geology of the continental shelf of north-west*
1262 *Europe. Heyden, London*, 216-235.

1263
1264 Van Der Zwaan, G.J. & Jorissen, F.J. 1991. Biofacial patterns in river-induced shelf anoxia.
1265 *Geological Society, London, Special Publications*, **58**, 65.

1266
1267 van Wees, J.D., Stephenson, R.A., Ziegler, P.A., Bayer, U., McCann, T., Dadlez, R., Gaupp, R.,
1268 Narkiewicz, M., *et al.* 2000. On the origin of the Southern Permian Basin, Central Europe. *Marine*
1269 *and Petroleum Geology*, **17**, 43-59, http://doi.org/http://dx.doi.org/10.1016/S0264-8172(99)00052-5.

1270
1271 Vespremeanu-Stroe, A., Preoteasa, L., Zăinescu, F., Rotaru, S., Croitoru, L. & Timar-Gabor, A. 2016.
1272 Formation of Danube delta beach ridge plains and signatures in morphology. *Quaternary*
1273 *International*, **415**, 268-285, http://doi.org/http://dx.doi.org/10.1016/j.quaint.2015.12.060.

1274
1275 Vollset, J. & Doré, A.G. 1984. A revised Triassic and Jurassic lithostratigraphic nomenclature for the
1276 Norwegian North Sea. *Norwegian Petroleum Directorate, Bull.*, **3**, 1-51.

1277
1278 Widess, M.B. 1973. How thin is a thin bed? *GEOPHYSICS*, **38**, 1176-1180,
1279 http://doi.org/10.1190/1.1440403.

1280
1281 Zhang, J.-J., Wu, S.-H., Fan, T.-E., Fan, H.-J., Jiang, L., Chen, C., Wu, Q.-Y. & Lin, P. 2016.
1282 Research on the architecture of submarine-fan lobes in the Niger Delta Basin, offshore West Africa.
1283 *Journal of Palaeogeography*, **5**, 185-204, http://doi.org/http://dx.doi.org/10.1016/j.jop.2016.05.005.

1284
1285 Zhuo, H., Wang, Y., Shi, H., Zhu, M., He, M., Chen, W. & Li, H. 2014. Seismic geomorphology,
1286 architecture and genesis of Miocene shelf sand ridges in the Pearl River Mouth Basin, northern South
1287 China Sea. *Marine and Petroleum Geology*, **54**, 106-122,
1288 http://doi.org/http://dx.doi.org/10.1016/j.marpetgeo.2014.03.002.

Ziegler, P.A. 1992. North Sea Rift System. *Tectonophysics*, **208**, 55-75.

Figure 1

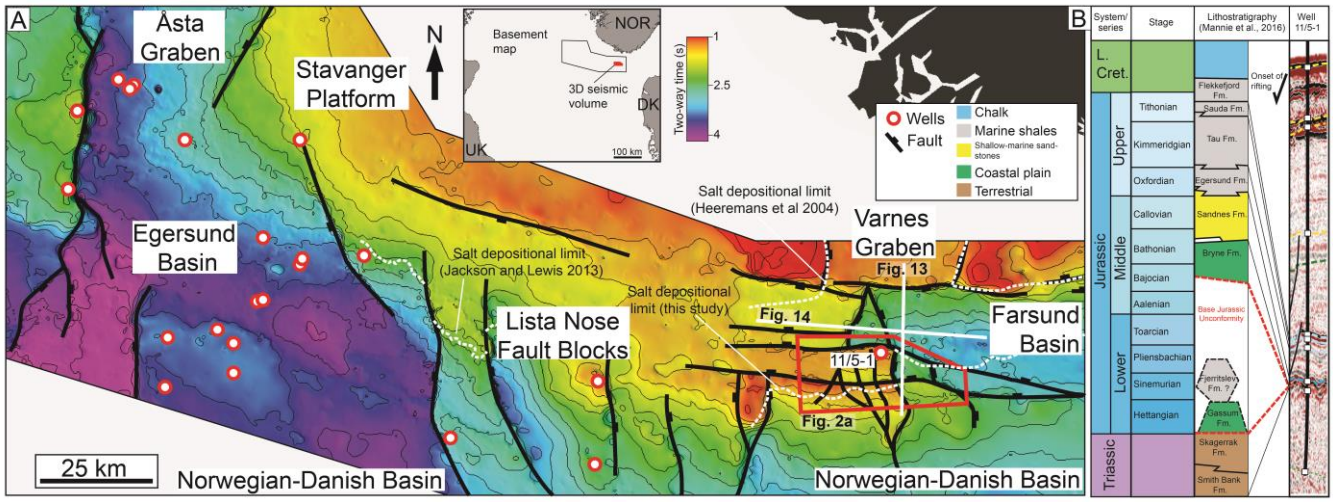
A
Åsta Graben
Stavanger Platform
Egersund Basin
Lista Nose Fault Blocks
Varnes Graben
Fig. 13
Farsund Basin
Fig. 14
11/5-1
Fig. 2a
Salt depositional limit (Heeremans et al 2004)
Salt depositional limit (Jackson and Lewis 2013)
Salt depositional limit (this study)
N
Basement map
NOR
3D seismic volume
DK
UK
100 km
Two-way time (s)
1
2.5
4
Wells
Fault
Chalk
Marine shales
Shallow-marine sand-stones
Coastal plain
Terrestrial
25 km
Norwegian-Danish Basin
Norwegian-Danish Basin
B
System/ series
Stage
Lithostratigraphy (Mannie et al., 2016)
Well 11/5-1
L. Cret.
Jurassic
Upper
Middle
Lower
Triassic
Tithonian
Kimmeridgian
Oxfordian
Callovian
Bathonian
Bajocian
Aalenian
Toarcian
Pliensbachian
Sinemurian
Hettangian
Flekkefjord Fm.
Sauda Fm.
Tau Fm.
Egersund Fm.
Sandnes Fm.
Bryne Fm.
Base Jurassic Unconformity
Ferritslev Fm. ?
Gassum Fm.
Skagerrak Fm.
Smith Bank Fm.
Onset of rifting

Figure 2

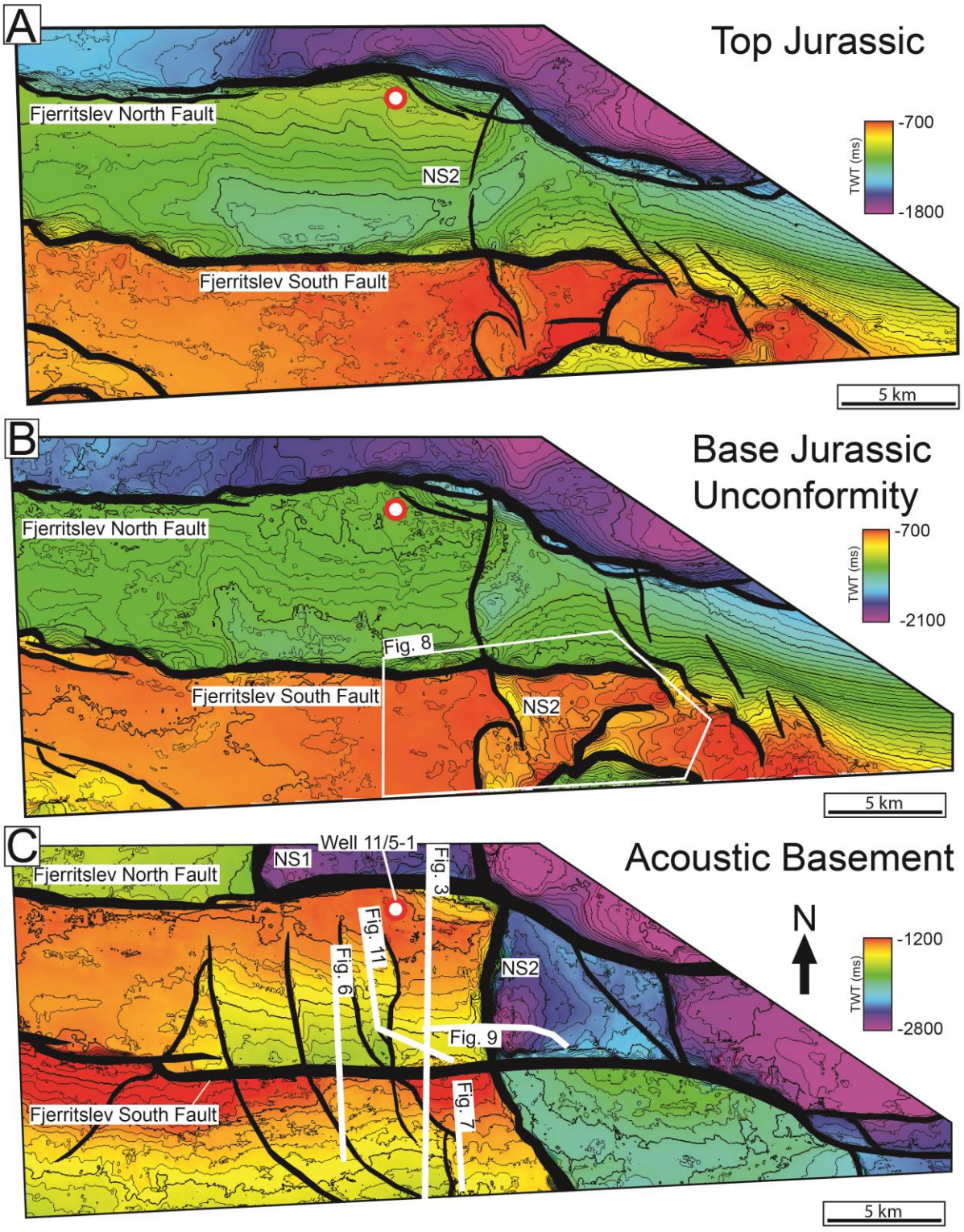
A
Top Jurassic
Fjerritslev North Fault
NS2
Fjerritslev South Fault
TWT (ms)
-700
-1800
5 km
B
Base Jurassic
Unconformity
Fjerritslev North Fault
Fig. 8
Fjerritslev South Fault
NS2
TWT (ms)
-700
-2100
5 km
C
Acoustic Basement
Well 11/5-1
NS1
Fjerritslev North Fault
Fig. 3
Fig. 11
Fig. 6
NS2
Fig. 9
Fig. 7
Fjerritslev South Fault
N
TWT (ms)
-1200
-2800
5 km

Figure 3

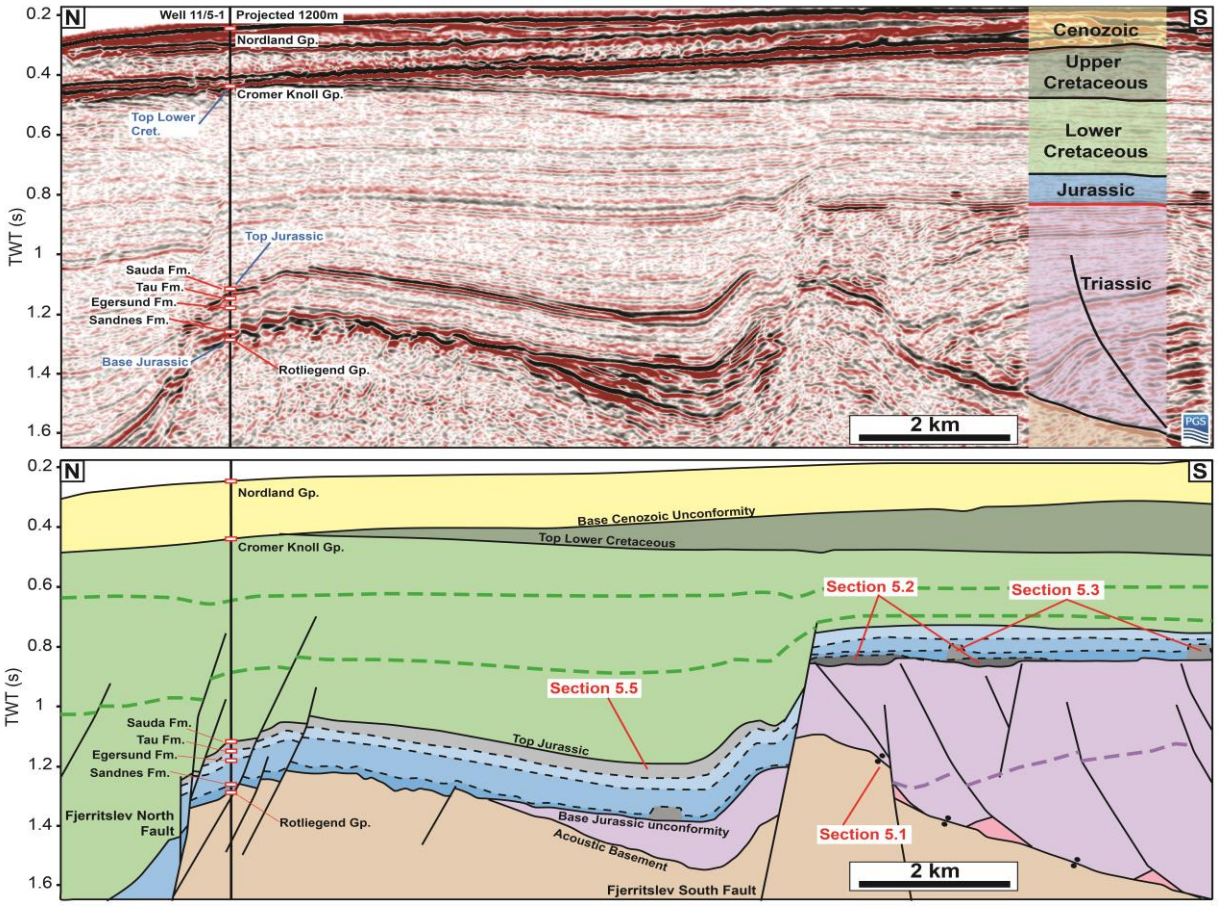
N
S
Well 11/5-1
Projected 1200m
Nordland Gp.
Cromer Knoll Gp.
Top Lower Cret.
Top Jurassic
Sauda Fm.
Tau Fm.
Egersund Fm.
Sandnes Fm.
Base Jurassic
Rotliegend Gp.
Cenozoic
Upper Cretaceous
Lower Cretaceous
Jurassic
Triassic
2 km
TWT (s)
Base Cenozoic Unconformity
Top Lower Cretaceous
Section 5.2
Section 5.3
Section 5.5
Section 5.1
Fjerritslev North Fault
Base Jurassic unconformity
Acoustic Basement
Fjerritslev South Fault

Figure 4

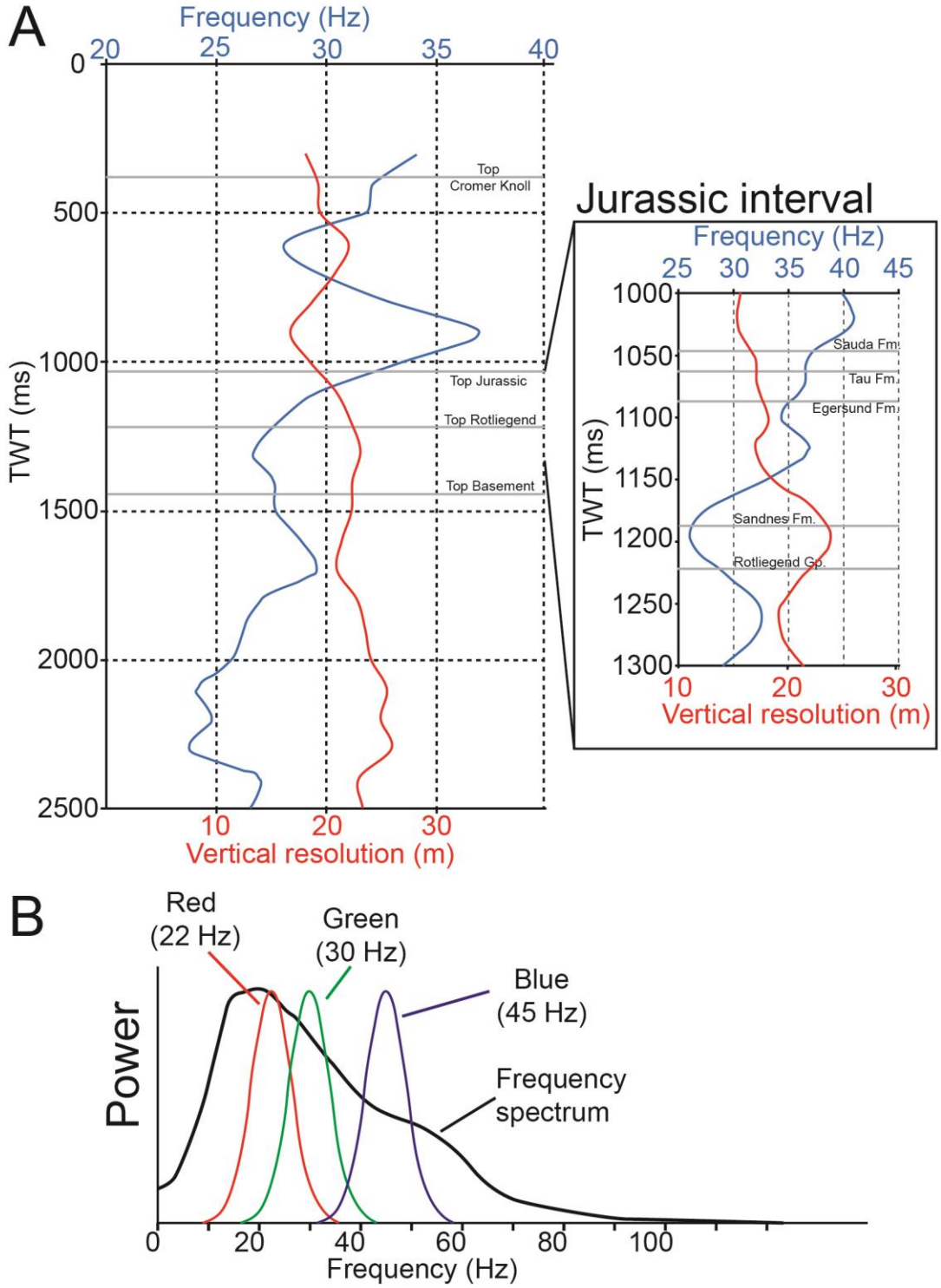
A
Frequency (Hz)
20
25
30
35
40
0
500
1000
1500
2000
2500
TWT (ms)
Top
Cromer Knoll
Top Jurassic
Top Rotliegend
Top Basement
10
20
30
Vertical resolution (m)
Jurassic interval
Frequency (Hz)
25
30
35
40
45
1000
1050
1100
1150
1200
1250
1300
TWT (ms)
Sauda Fm.
Tau Fm.
Egersund Fm.
Sandnes Fm.
Rotliegend Gp.
10
20
30
Vertical resolution (m)
B
Red
(22 Hz)
Green
(30 Hz)
Blue
(45 Hz)
Frequency
spectrum
Power
0
20
40
60
80
100
Frequency (Hz)

Figure 5

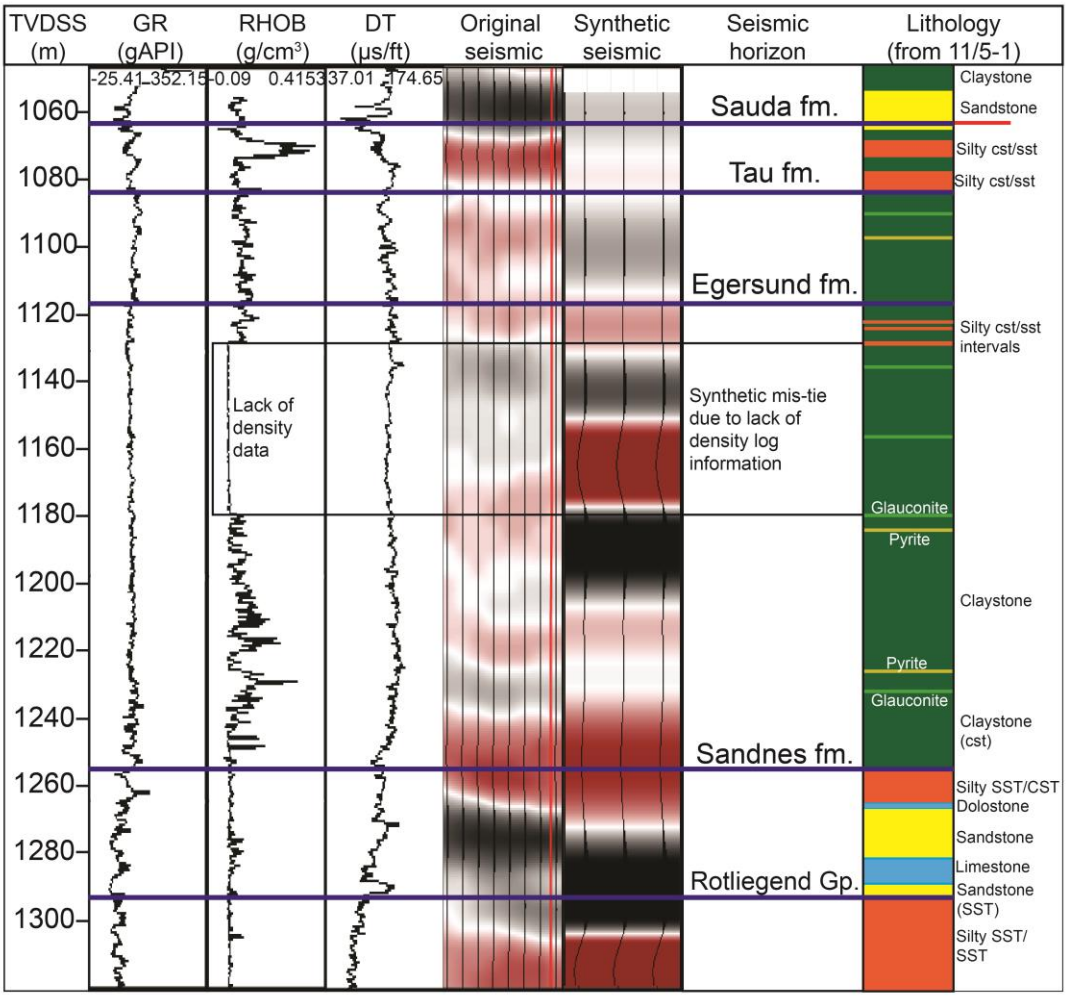
TVDSS (m)
GR (gAPI)
RHOB (g/cm³)
DT (µs/ft)
Original seismic
Synthetic seismic
Seismic horizon
Lithology (from 11/5-1)
-25.41 352.15
-0.09 0.4153
37.01 174.65
1060
1080
1100
1120
1140
1160
1180
1200
1220
1240
1260
1280
1300
Sauda fm.
Tau fm.
Egersund fm.
Sandnes fm.
Rotliegend Gp.
Lack of density data
Synthetic mis-tie due to lack of density log information
Claystone
Sandstone
Silty cst/sst
Silty cst/sst
Silty cst/sst intervals
Glauconite
Pyrite
Claystone
Pyrite
Glauconite
Claystone (cst)
Silty SST/CST
Dolostone
Sandstone
Limestone
Sandstone (SST)
Silty SST/ SST

Figure 6

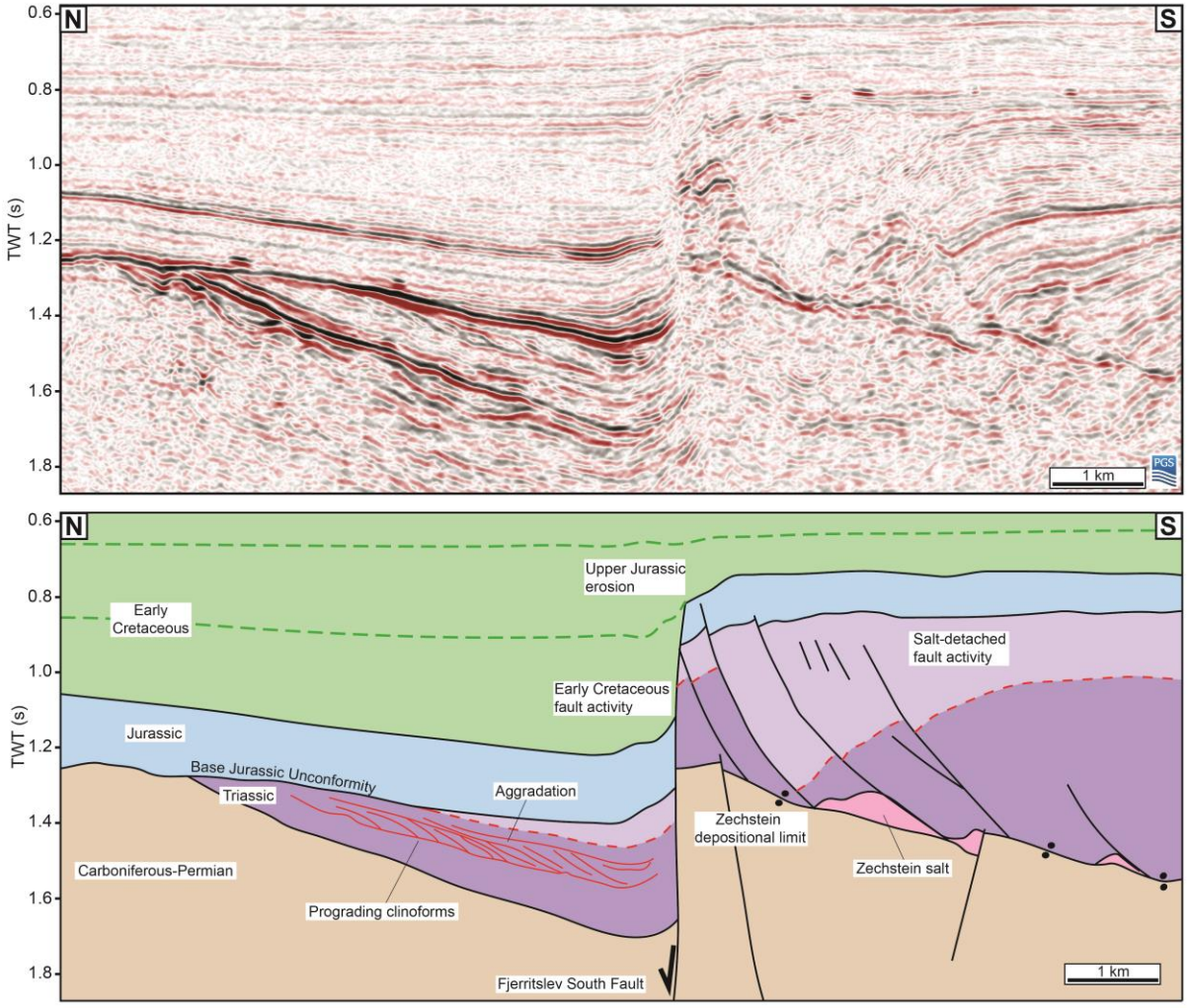
N
S
TWT (s)
0.6
0.8
1.0
1.2
1.4
1.6
1.8
1 km
PGS
Upper Jurassic erosion
Early Cretaceous
Salt-detached fault activity
Early Cretaceous fault activity
Jurassic
Base Jurassic Unconformity
Triassic
Aggradation
Zechstein depositional limit
Zechstein salt
Carboniferous-Permian
Prograding clinoforms
Fjerritslev South Fault

Figure 7

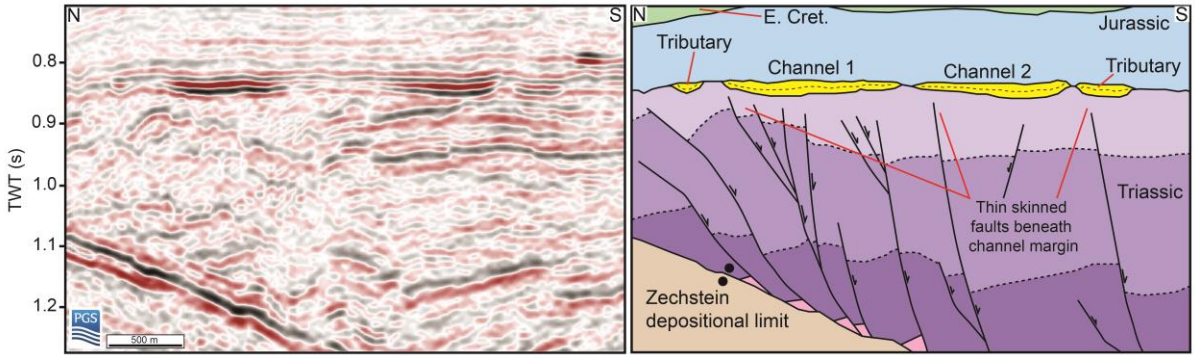
N
S
0.8
0.9
1.0
1.1
1.2
TWT (s)
PGS
500 m
N
E. Cret.
Jurassic
S
Tributary
Channel 1
Channel 2
Tributary
Triassic
Thin skinned
faults beneath
channel margin
Zechstein
depositional limit

Figure 8

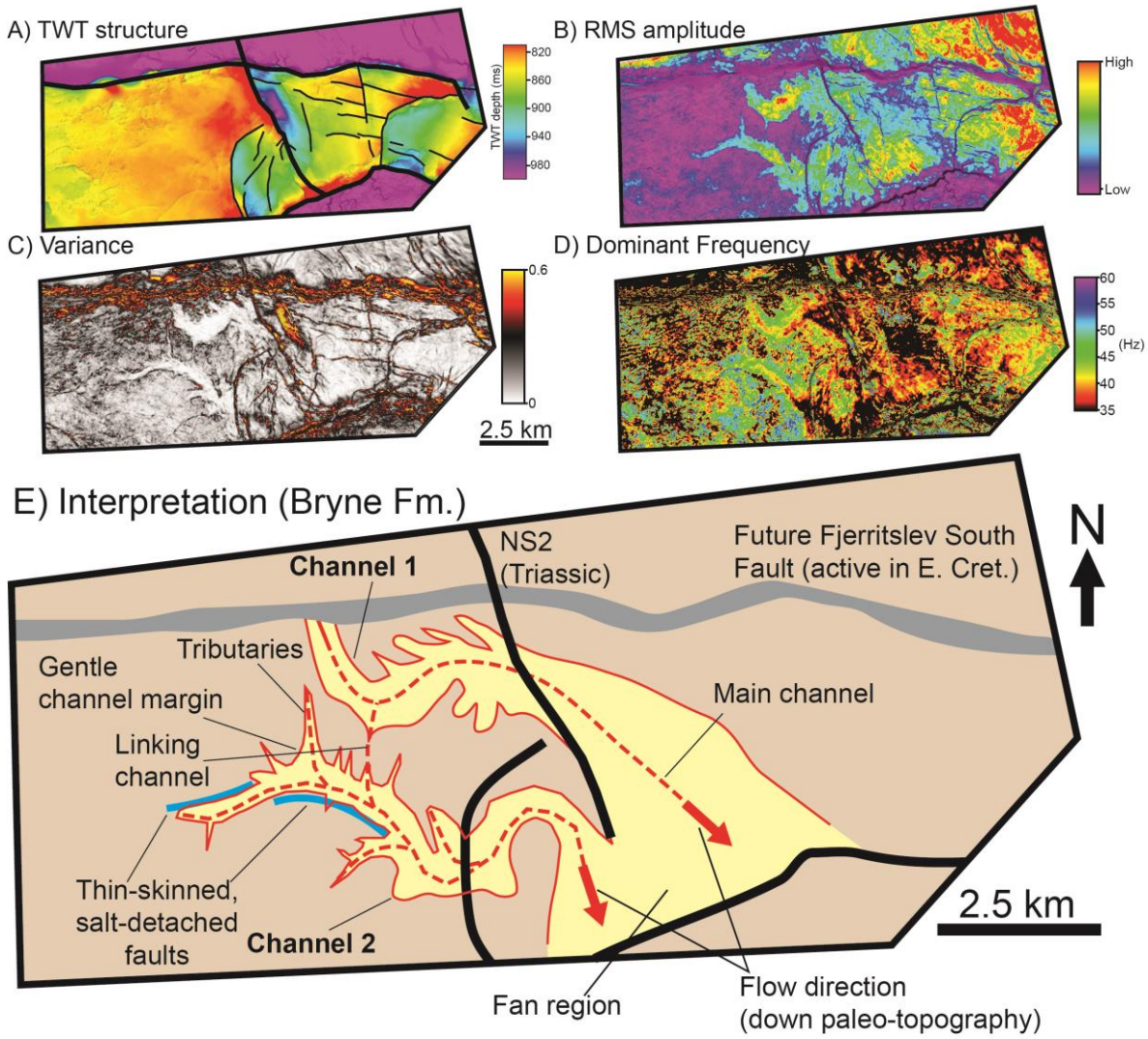
A) TWT structure
TWT depth (ms)
820
860
900
940
980
B) RMS amplitude
High
Low
C) Variance
0.6
0
2.5 km
D) Dominant Frequency
60
55
50
45
40
35
(Hz)
E) Interpretation (Bryne Fm.)
Channel 1
NS2
(Triassic)
Future Fjerritslev South
Fault (active in E. Cret.)
N
Tributaries
Gentle
channel margin
Linking
channel
Main channel
Thin-skinned,
salt-detached
faults
Channel 2
2.5 km
Fan region
Flow direction
(down paleo-topography)

Figure 9

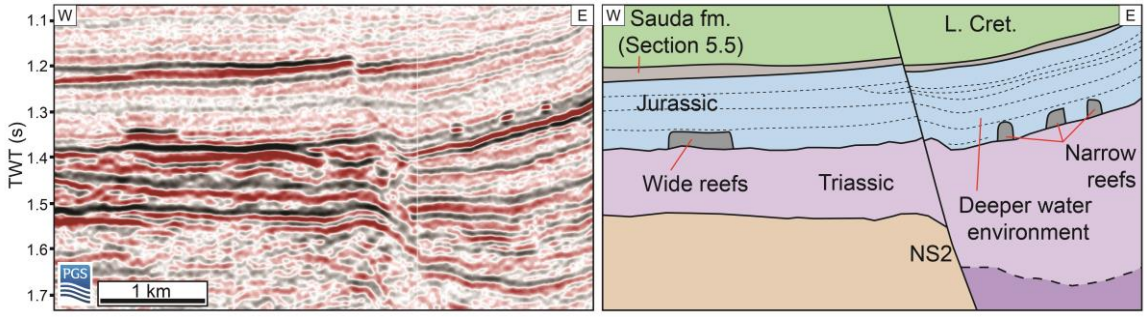
W
E
1.1
1.2
1.3
1.4
1.5
1.6
1.7
TWT (s)
PGS
1 km
W
Sauda fm.
(Section 5.5)
L. Cret.
E
Jurassic
Wide reefs
Triassic
Narrow
reefs
Deeper water
environment
NS2

Figure 10

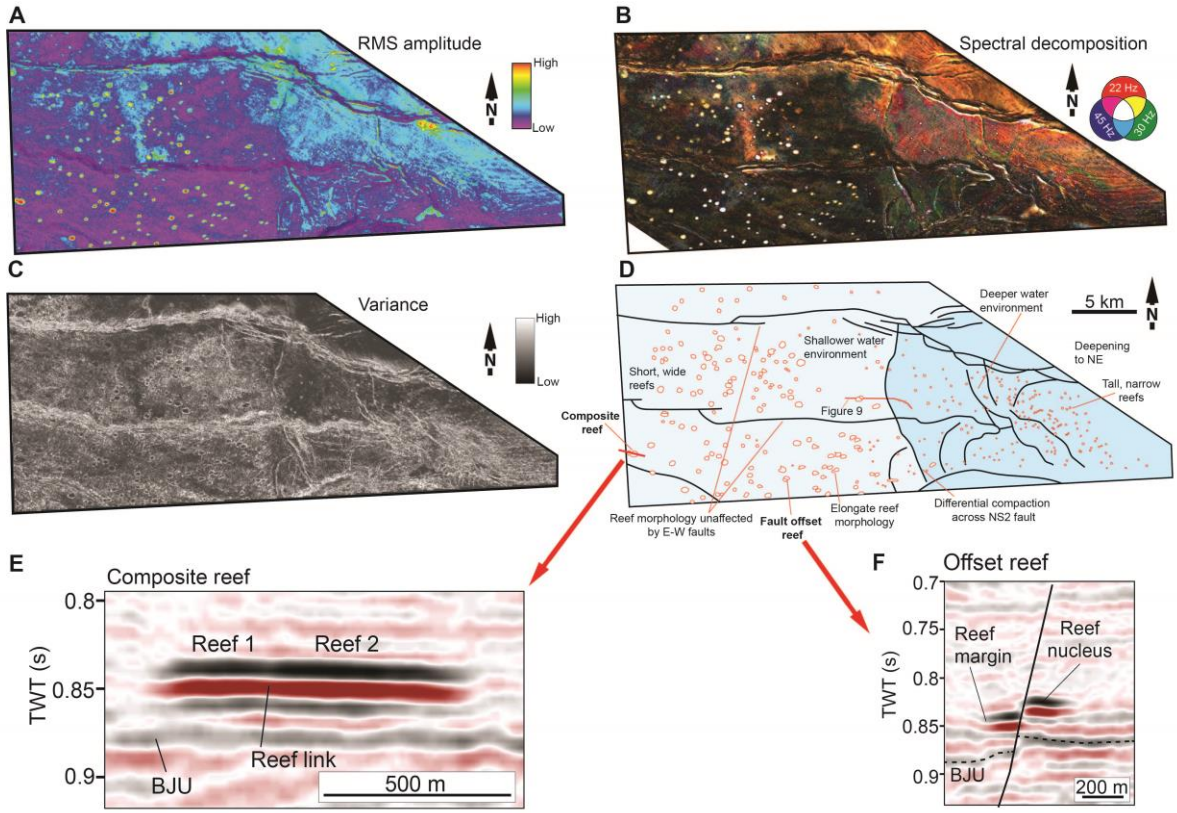
A
RMS amplitude
High
Low
N
B
Spectral decomposition
22 Hz
45 Hz
30 Hz
N
C
Variance
High
Low
N
D
Deeper water environment
5 km
N
Shallower water environment
Deepening to NE
Short, wide reefs
Tall, narrow reefs
Figure 9
Composite reef
Reef morphology unaffected by E-W faults
Fault offset reef
Elongate reef morphology
Differential compaction across NS2 fault
E
Composite reef
TWT (s)
0.8
0.85
0.9
Reef 1
Reef 2
Reef link
BJU
500 m
F
Offset reef
TWT (s)
0.7
0.75
0.8
0.85
0.9
Reef margin
Reef nucleus
BJU
200 m

Figure 11

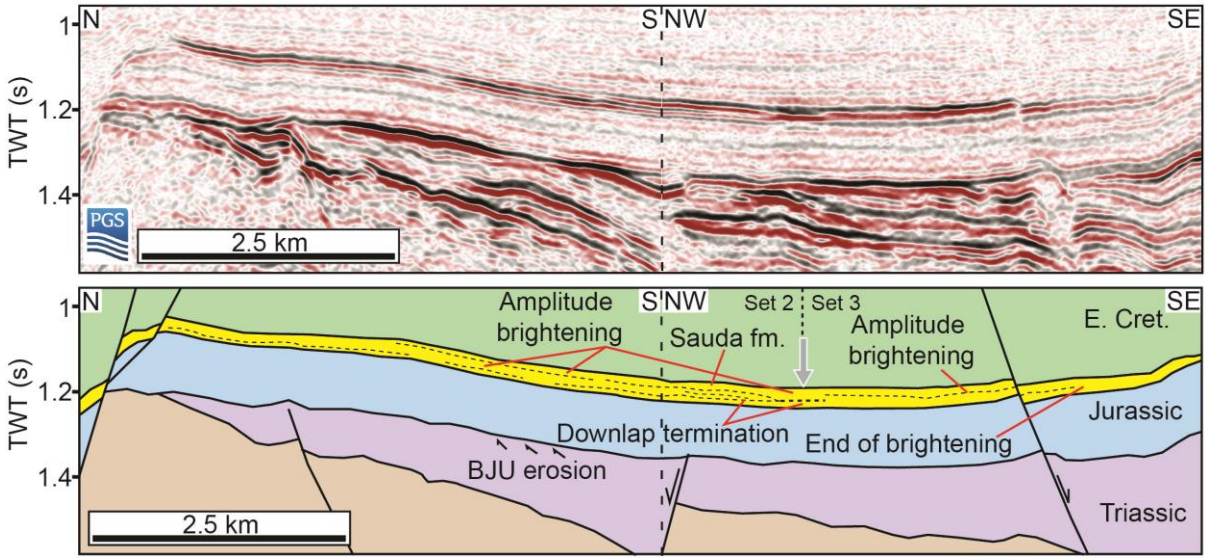
N
S
NW
SE
TWT (s)
1
1.2
1.4
PGS
2.5 km
Amplitude brightening
Sauda fm.
Set 2
Set 3
Amplitude brightening
E. Cret.
Jurassic
Downlap termination
End of brightening
BJU erosion
Triassic

Figure 12

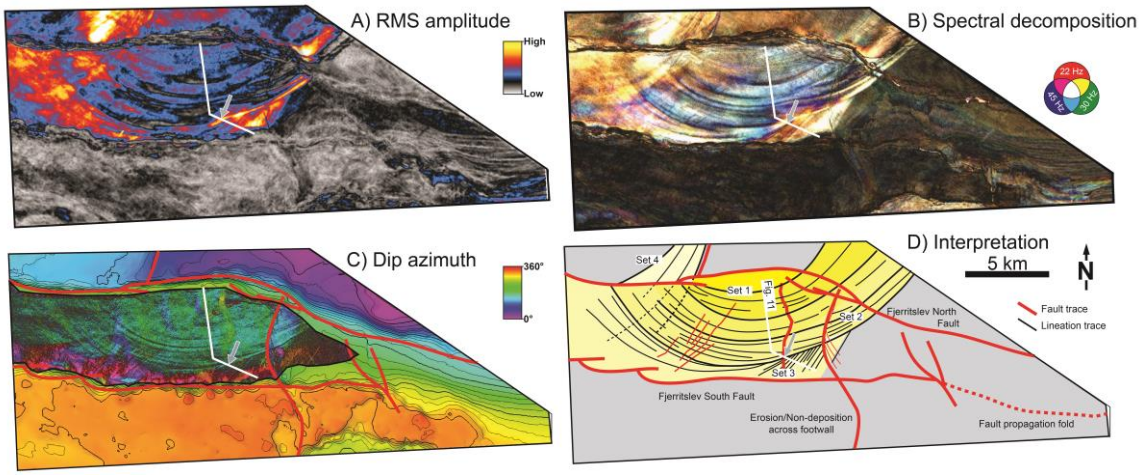
A) RMS amplitude
High
Low
B) Spectral decomposition
22 Hz
45 Hz
90 Hz
C) Dip azimuth
360°
0°
D) Interpretation
5 km
N
Set 4
Set 1
Fig. 11
Set 2
Set 3
Fjerritslev North Fault
Fjerritslev South Fault
Erosion/Non-deposition across footwall
Fault propagation fold
Fault trace
Lineation trace

Figure 13

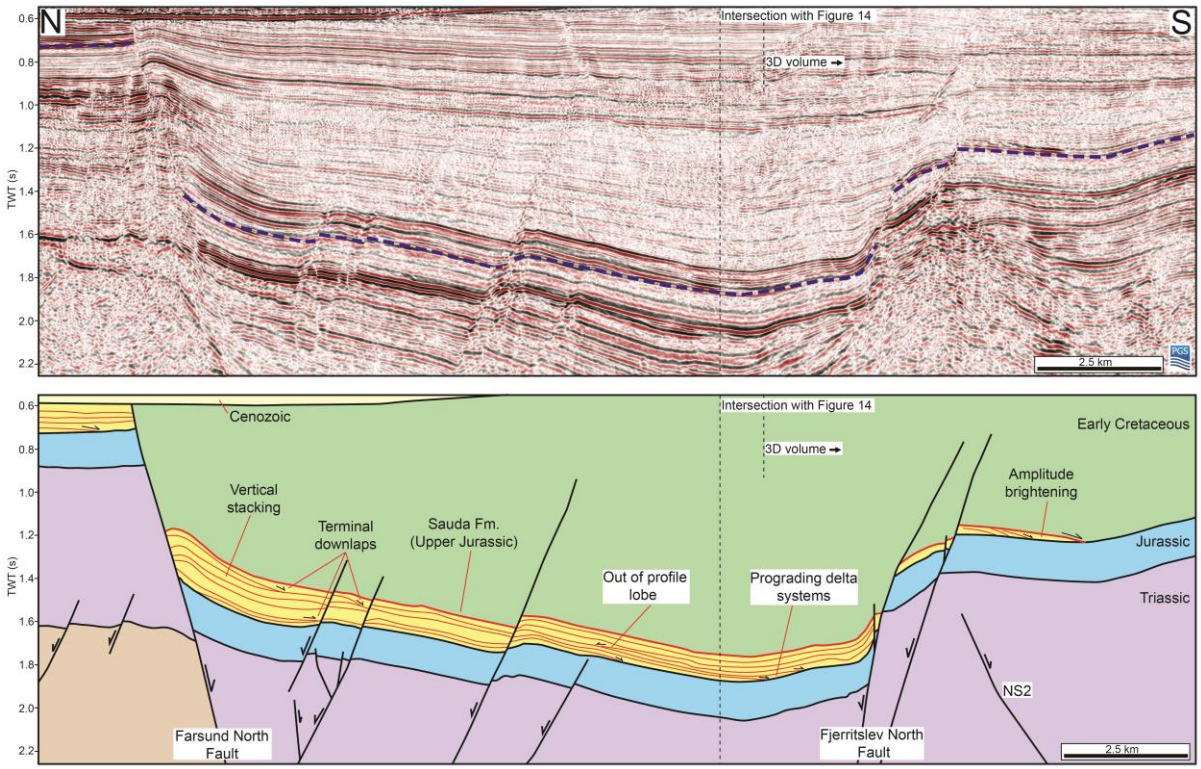
N
S
Intersection with Figure 14
3D volume
TWT (s)
2.5 km
Cenozoic
Vertical stacking
Terminal downlaps
Sauda Fm. (Upper Jurassic)
Out of profile lobe
Prograding delta systems
Amplitude brightening
Early Cretaceous
Jurassic
Triassic
NS2
Farsund North Fault
Fjerritslev North Fault

1333 **Figure 14**

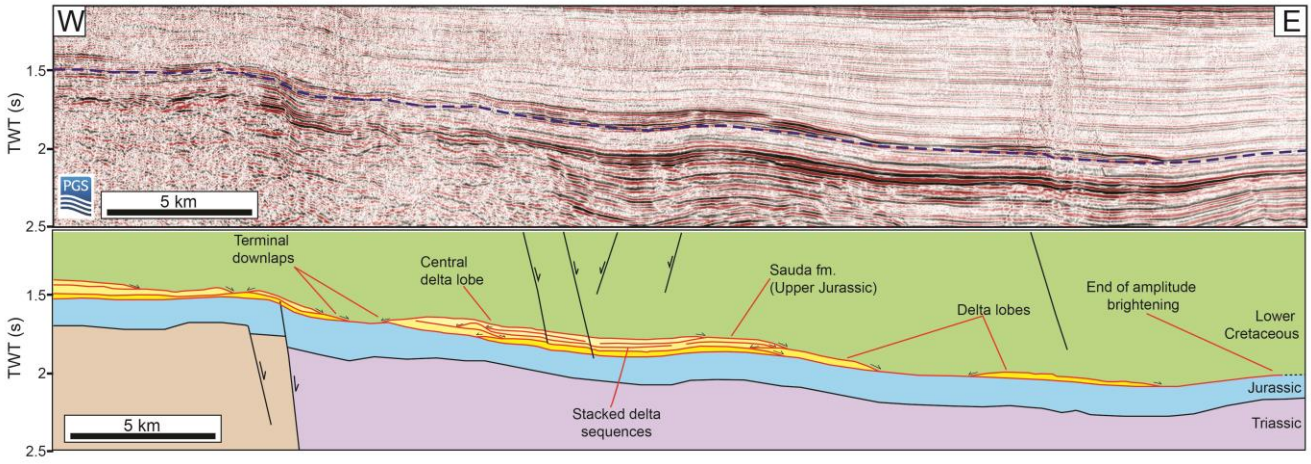

1334

1335

Figure 15

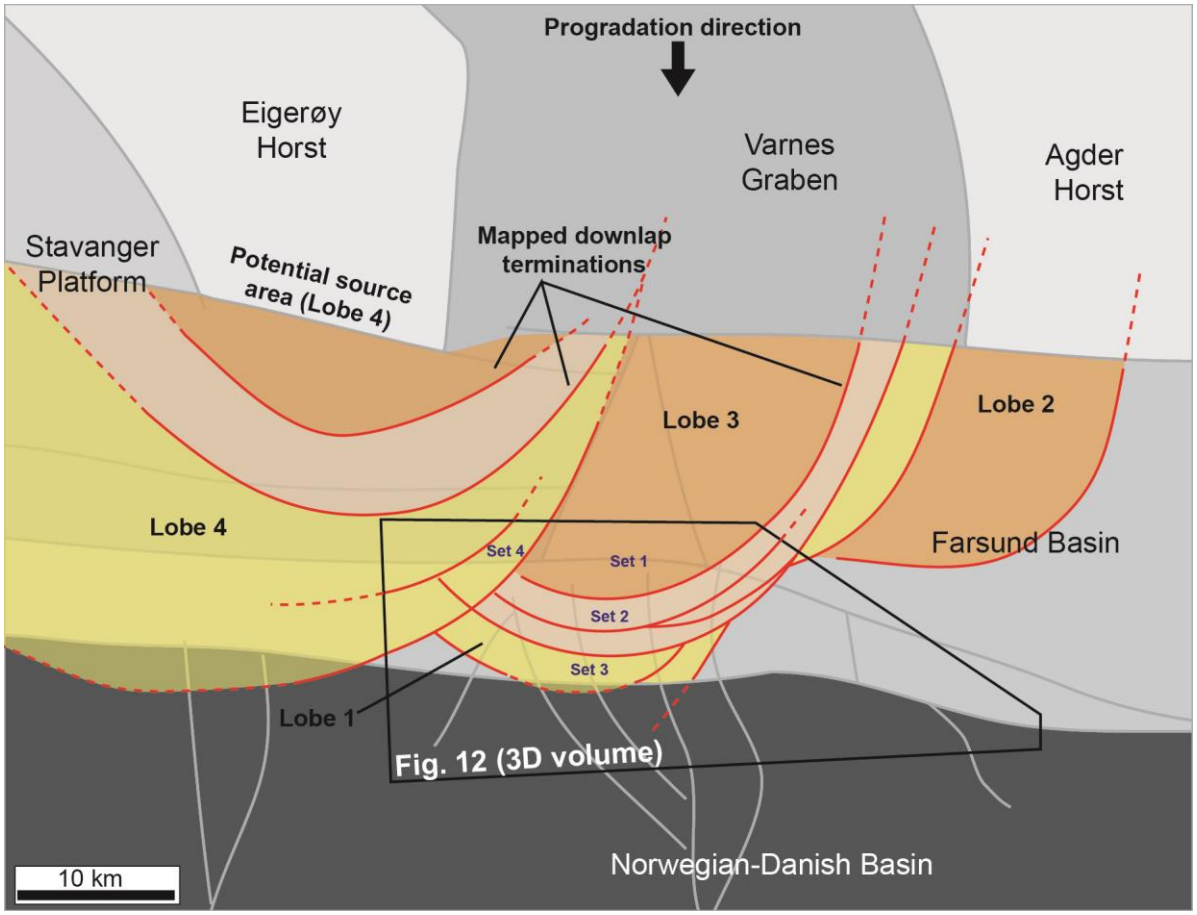
Progradation direction
Eigerøy
Horst
Varnes
Graben
Agder
Horst
Stavanger
Platform
Potential source
area (Lobe 4)
Mapped downlap
terminations
Lobe 3
Lobe 2
Lobe 4
Farsund Basin
Set 4
Set 1
Set 2
Set 3
Lobe 1
Fig. 12 (3D volume)
Norwegian-Danish Basin
10 km

Figure 16

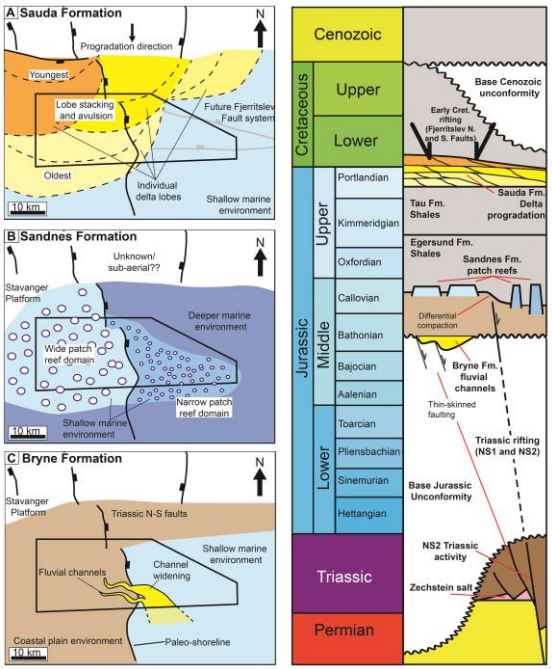
A Sauda Formation
N
Progradation direction
Youngest
Lobe stacking and avulsion
Future Fjerritslev Fault system
Oldest
Individual delta lobes
Shallow marine environment
10 km
B Sandnes Formation
Unknown/ sub-aerial??
Stavanger Platform
Deeper marine environment
Wide patch reef domain
Narrow patch reef domain
Shallow marine environment
10 km
C Bryne Formation
Stavanger Platform
Triassic N-S faults
Shallow marine environment
Fluvial channels
Channel widening
Coastal plain environment
Paleo-shoreline
10 km
Cenozoic
Cretaceous
Upper
Lower
Jurassic
Upper
Middle
Lower
Portlandian
Kimmeridgian
Oxfordian
Callovian
Bathonian
Bajocian
Aalenian
Toarcian
Pliensbachian
Sinemurian
Hettangian
Triassic
Permian
Base Cenozoic unconformity
Early Cret. rifting (Fjerritslev N. and S. Faults)
Sauda Fm. Delta progradation
Tau Fm. Shales
Egersund Fm. Shales
Sandnes Fm. patch reefs
Differential compaction
Bryne Fm. fluvial channels
Thin-skinned faulting
Triassic rifting (NS1 and NS2)
Base Jurassic Unconformity
NS2 Triassic activity
Zechstein salt

1343 **Figure 17**

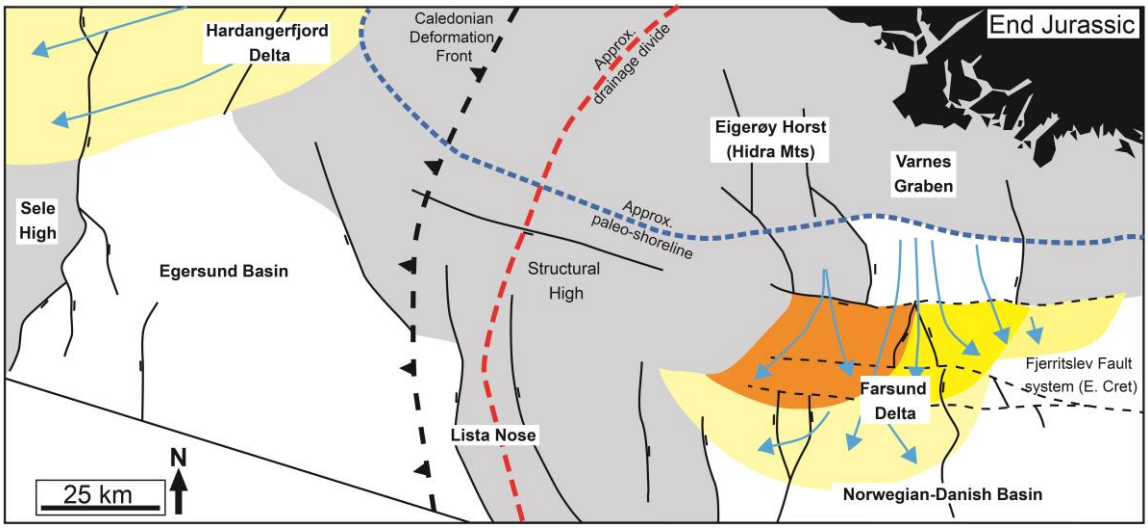

1344